Journal of Thermal Analysis and Calorimetry (2020) 140:1–32
https://doi.org/10.1007/s10973-019-08741-4

A study on thermohydraulic characteristics of fluid flow through microchannels

Jeet Prakash Sharma[1] · Aashish Sharma[2] · Ravindra D. Jilte[2] · Ravinder Kumar[2] · Mohammad Hossein Ahmadi[3]

Received: 30 May 2019 / Accepted: 19 August 2019 / Published online: 19 September 2019

Abstract

At present, miniaturization of the devices in order to make them for effective performance, reliability and ease at cost is the primary need of any nation. In this direction, the role of microchannels can play an important role in the further development of industrial growth. The increased demand of the microchips in the industrial areas has increased the number of transistors for the improved functionality which leads to the emission of the higher heat flux, which is already a big challenge in the electronic sector. In the present paper, a comprehensive review on microchannels has been done regarding single-phase and multi-phase studies. In the present paper, an intensive review of the thermal and hydraulic characteristics of fluid flow in microchannels at different hydraulic diameters and their effects on performance has been done. The effects of the various parameters such as the Reynolds number (Re), Nusselt number (Nu), friction factor (f), pressure drop (P), working fluid and cross-sectional geometry of duct, as well as the hydrodynamic and thermal aspects, has been also studied. It was concluded through the literature study that transition from laminar to turbulent is very much affected by channel cross-sectional geometry, aspect ratio, channel wall roughness and compressibility effects. Also, researchers only explored the laminar region for its pressure drop and heat transfer characteristics, while the turbulent flow regime is yet to be explored. It was observed that most of the correlation over-estimated the value of pressure drop in multi-phase flow.

Keywords Single-phase flow · Multi-phase flow · Microchannel · Minichannel · Heat transfer · Pressure drop

List of symbols

A	Area
Pw	Wetted perimeter
a	Channel height (m)
b	Channel width (m)
C	Lockhart–Martinelli parameter
C^*	Characteristics quantity
Co	Convective number
v	Velocity
L or l	Length
f	Friction factor
Re*	Laminar equivalent Reynolds number
F_{fl}	Fluid surface parameter
Pr	Prandtl number
h	Heat transfer coefficient (W m^{-2} K^{-1})
k	Thermal conductivity (W m^{-1} K^{-1})
Nu	Nusselt number
Pr	Prandtl number
T	Temperature (K)
We	Weber number
Ac	Area of cross section
Di	Internal diameter
BL	Boiling number
Bo	Bond number
C_{P}	Specific heat (J kg^{-1} K^{-1})
P_0	Poiseuille number
D_{h}	Hydraulic diameter (m)
D	Diameter (internal)
$k(x)$	Hagenbach factor
Fr	Froude number
G	Mass velocity (kg m^{-2} s^{-1})
Nu	Nusselt number
J	Total mixture volumetric flux (m s^{-1})

✉ Ravinder Kumar
rav.chauhan@yahoo.co.in

✉ Mohammad Hossein Ahmadi
mohammadhosein.ahmadi@gmail.com

[1] Department of Mechanical Engineering, Lovely Professional University, Phagwara, Punjab, India

[2] Faculty of Mechanical Engineering, Lovely Professional University, Phagwara, Punjab, India

[3] Faculty of Mechanical Engineering, Shahrood University of Technology, Shahrud, Iran

Ma	Mach number
P	Pressure (Pa)
Re	Reynolds number
U	Velocity (m s^{-1})

Greek symbols

τ	Shear stress (Pa)
μ	Dynamic viscosity (Pa s^{-1})
ρ	Density (kg m^{-3})
α	Channel aspect ratio
λ	Laplace constant
α	Aspect ratio
e	Roughness of the pipe
κ	Hagenbach factor
$\emptyset_{LO}$	Two-phase multiplier (for liquids only)
σ	Surface tension (N m^{-1})

Subscripts

app	Apparent
crit	Critical
tot	Total
TP	Two-phase mixture
sat	Saturated
Exp	Experimental
FD	Fully developed
L	Liquid
V	Vapor

Introduction

The microchannel heat exchanger is the 'heat exchanger of next generation,' the new technology which can provide the solution for the cooling of high-heat flux problem. Microchannels possess the ability of high heat transfer rate because of their large surface area-to-volume ratio, which makes them the finest choice for the development of the microheat exchangers used for the cooling of electronic and aerospace components. There are many applications of the microchannels in industrial sectors but not limited to electronic, automobile, aerospace and cryosurgery area. Microchannels have attracted the minds of researchers because of its wide applications in various areas like electronic devices, automobile, aerospace, fuel processor and nuclear reactors. Microchannels serve as the sole component in order to build the microheat exchangers which apparently are seen as the heat exchangers of the next generation because of their application advantages as well as their efficiency. To enhance the thermal and hydraulic performance of the microchannels, various studies on both numerical and experimental works have been carried out in the past years for single-phase and multi-phase fluid flows. Basically, the cooling is done in two ways: the air cooling or the water cooling. When the requirement of cooling passes over 100 W cm^{-2}, then the cooling of system is not feasible using air or water for flowing fluids. In several applications, when components of the system require to remove the heat flux of higher order, then it becomes difficult to use a larger heat sink, probably lager than component itself. It has already provided a new platform for researchers to develop a new kind of heat sinks that can be incorporated with the heat source for the removal of the heat flux. These heat sinks are made of silicon material, and a layer of silicon oxide is kept over them for the electrical insulation. Quite narrow microchannels of different shapes such as rectangular, circular or triangular are framed around using fins to increase the rate of heat removal by flowing the cold fluid (coolant) through these microchannels. Tuckerman and Pease [1] explained the idea of using microchannel heat sinks to investigate the single-phase forced convective heat transfer. It was stated that it could potentially remove heat flux up to 1000 W cm^{-2}. The value of the convection heat transfer coefficient (h) was found to be an obstacle to obtain low thermal resistance value. It was seen that for laminar flow, the value of 'h' is inversely proportional to the width of the channel. However, the high aspect ratio (w H^{-1}) will, in turn, increase the surface area which reduces the value of thermal resistance to provide a high rate of heat transfer. Philips [2] performed an experiment on microchannel heat sinks that are used for the applications in microelectronics such as laser diodes and for high-energy laser mirrors. To cool the laser diode, heat sinks are made with indium phosphide having a thermal resistance of 0.072 °C W^{-1} cm^{-2}, which can dissipate the heat flux of 1000 W cm^{-2}. Hahn et al. [3] investigated the packaging of high-powered multi-chip modules, basically focused on the three major areas: (1) fabrication of multi-chip module, (2) development of high-performance microchannel heat sinks and (3) assembling technology having very low thermal performance. A thermostat module having a size of 2 × 2 inches is capable of heat dissipation of hundreds of watts. Thermal resistance value was maintained below 0.6 K cm^{-2} W^{-1} at a heat flux of 50 W cm^{-2}. Martin et al. [4] investigated microchannel heat exchangers which were designed for the cooling of heat flux of order 100 W cm^{-2}. Each section had 150 microchannels having dimensions of 100 μm deep, 100 μm wide and space 50–100 μm. It was found that the thermal capacity of the crystal board was 20 W and 15 W at the crystal temperature of 90 °C and 70 °C, respectively. It was observed that at the flow rate of 50 g s^{-1} of water, the system provides an efficient cooling of 0.6 × 105 W m^{-2} K^{-1} [5]. Studies have observed that the heat sink incorporating

microchannel has been known for the collective heat flux removal of up to 500 W cm^{-2} used in the cooling of laser diode array [6–8]. The basic governing equations related to fluid flow in conventional channels are given below [9]:

Conservation of mass

$$\nabla \cdot \left(\rho_{\mathrm{m}} \vec{V}_{\mathrm{m}}\right) = 0 \tag{1}$$

Conservation of momentum

$$\nabla \cdot \left(\rho_{\mathrm{m}} \vec{V}_{\mathrm{m}} \vec{V}_{\mathrm{m}}\right) = -\nabla \cdot P + \nabla \cdot [\tau - \tau_{\mathrm{t}}] + \nabla \cdot \left[\sum_{k-1}^{n} \phi_{\mathrm{k}} \rho_{\mathrm{k}} \vec{V}_{\mathrm{dr,k}} \vec{V}_{\mathrm{dr,k}}\right] \tag{2}$$

where

$$\tau = \mu_{\mathrm{m}} \nabla \cdot \vec{V}_{\mathrm{m}} \text{ and } \tau_{\mathrm{t}} = \sum_{\mathrm{k}-1}^{n} \left[\phi_{\mathrm{k}} \rho_{\mathrm{k}} \vec{v_{\mathrm{k}}} \vec{v_{\mathrm{k}}}\right]$$

Conservation of energy

$$\nabla \cdot \sum_{k-1}^{n} \left\{\phi_{\mathrm{k}} \vec{V}_{\mathrm{k}} (\rho_{\mathrm{k}} H_{\mathrm{k}} + P)\right\} = \nabla \cdot \left(\lambda_{\mathrm{eff}} \nabla T + C_{\mathrm{P}} \rho_{\mathrm{m}} \vec{vt}\right) \tag{3}$$

The classification criteria of the microchannels were proposed by many researchers over the years according to the various parameters. Serizawa et al. [10] defined the criteria for the microchannel and defined the Laplace constant should be greater than or equal to the microchannel diameter as given below.

$$\lambda \geq D_{\mathrm{h}} \tag{4}$$

where 'λ' is the Laplace constant and the 'D_{h}' is the microchannel hydraulic diameter. Another classification was given by Mehendale et al. [11] and they classified microchannels on the basis of its hydraulic diameter (see Table 1). Kandlikar and Grande [12] also classified the microchannels on the same basis as shown in Table 2.

Microchannels were defined by Palm [13] as an element or means of heat transfer which does not directly follow the classical theories of heat transfer or fluid flow. Thus, the flow characteristics such as friction factor and the heat transfer characteristics cannot be easily predicted. A study

Table 1 Classification of microchannels [11]

Classification	Hydraulic diameter
Microheat exchangers	$1\,\mu m \leq D_{\mathrm{h}} \leq 100\,\mu m$
Macro-heat exchangers	$100\,\mu m \leq D_{\mathrm{h}} \leq 1$ mm
Compact heat exchangers	$1\,\mathrm{mm} \leq D_{\mathrm{h}} \leq 6\,\mathrm{mm}$
Conventional heat exchangers	$D_{\mathrm{h}} \leq 6\,\mathrm{mm}$

Table 2 Classification of channels [12]

Classification	Hydraulic diameter
Microchannels	$10\,\mu m \leq D_{\mathrm{h}} \leq 200\,\mu m$
Minichannels	$200\,\mu m \leq D_{\mathrm{h}} \leq 3$ mm
Conventional channels	$D_{\mathrm{h}} \geq 6$ mm

by Stefan [14] used a microscale-sized system which does not show the same typical observations as the macro-sized systems and stated that it is not appropriate to differentiate the microchannels and minichannels on the basis of a specific diameter. The investigation performed by Halelfadl et al. [15] mainly concentrated on the analytical optimization of heat sink incorporated with rectangular microchannels using the water-based solution of nanofluids as a coolant. The results of the study demonstrated that using nanofluids as working fluids has reduced the value of overall thermal resistance and it can increase the thermal performance of the flowing fluid while dealing at large temperature. A study by Warrier et al. [16] investigated a two-phase cooling system incorporating microchannels which also had the side wall for the purpose of reducing the high heat fluxes in semiconductor devices. Yu et al. [17] investigated the thermal characteristics as well as the hydraulic characteristics of the fractal tree-shaped microchannels having various aspect ratios. The range of Reynolds number was set between 150 and 1200. The results of the investigation proposed that microchannels with fractal tree-shaped geometry had much larger heat transfer coefficient as compared to the straight microchannels. The same treelike thermal performance of microchannels was also investigated [18–21]. Chamkha et al. [22, 23] numerically investigated the fully developed free and mixed conventions in vertically oriented channel. Results of the study show that for a fixed value of R, the material parameter gets reduced to the velocity profile in free convection and velocity and microporation profiles become distorted in developing region of mixed convention. The study also investigated hydromagnetic two-phase flow [24] and reported that the flow rate of fluid and particle phase get reduced due to the presence of the particles in the channel and the volumetric flow rates and the skin friction coefficients decrease as the Hartmann number increases. Chamkha [25–28] also investigated various areas such as unsteady laminar hydromagnetic flow and heat transfer characteristics in channels, porous channels and vertical channels with wall heating conditions and reviewed the application of nanofluids in microchannels. The magneto hydrodynamic flow in a vertical microchannel using the Al_2O_3–water-based nanofluid was analyzed by Ibáñez et al. [29]. They

concluded that the nanoparticle volume fraction and slip length reach the higher value, when the permeability increases, while the global entropy generation is at its minimum value, and they reach the minimum value when the global entropy generation decreases. Shashi kumar et al. [30] investigated the entropy generation in microchannels using nanofluids with partial slips and convective conditions. It observed that the entropy generation was higher in $Ti_6Al_4VH_2O$ nanofluid as compared to AA7075-H_2O. In the study performed by Khodabandeh et al. [31], they showed that microchannel heat sink design with sinusoidal cavities and rectangular ribs can increase the Nusselt number and heat transfer.

The effects of the flow fluctuation during boiling and periodic reversed flow were studied [21, 32–38] and stated that the thermal performance of the microchannel used as an evaporator in an air-conditioning system may create a problem. Tuo and Hrnjak [21] proposed a bright solution of the problem to decrease these effects to a significant level by using the ventilation system and also by altering the route of backflow vapor collected at the header at the inlet. Moallem et al. [39] performed an experiment on the microchannel heat exchanger incorporated with louvered fins and the effects of frost formation. The results of the experiment concluded that the temperature of the fin surface and the air humidity were the primary parameters which affect mostly the rapid growth rate of frost at a particular dry bulb temperature of the air. The performance of the cyclic frosting and defrosting for two different types of microheat exchangers was also experimented and studied by Xu et al. [40] and Liu et al. [41]. There were several other similar studies that have used microchannels and various conditions to increase the thermal performance of the microchannel heat exchangers [42–53]. In another study by Morini et al. [54], they explained a heat sink. Using the numerical investigation, Sarangi et al. [55] developed a numerical model of boiling heat transfer by using microchannels. They focused on the phenomenon of forced convection in two-phase fluid flow in microchannels and used water as working fluid. Flat microtubes made of aluminum materials remained the center of attention for many years. In majority, it was used in designing the air-conditioning systems and in the refrigeration industries where high cooling is required [56–63]. Zhang et al. [56] performed both experimental and numerical works on a bent plane consisting of flat microchannel tubes. The conclusion of the study described that under normal working conditions, the degradation of the microchannels is very small.

In the last past few years, research on the determination of convective heat transfer and pressure drop in mini- and microchannels has been conducted at a rapid rate [64–67]. Szczukiewicz et al. [64] evaluated the heat transfer coefficient of some refrigerants used in evaporator consist of multiple microchannels. It was concluded that two-phase flow heat sink which has microgap possesses very effective capability to lower the disadvantages associated with the normal heat sink of two-phase flow, mainly of that heat sink which shows some flow instabilities, a reversal inflow and the variation in wall temperatures between the microchannels. Another experiment performed by Alam et al. [65] investigated the characteristics of fluid flow and heat transfer in a microgap heat sink while using deionized water as flowing fluid. The results of this study were compared with the results obtained from the investigation performed over the normal microchannel heat sink. Fani et al. [66] performed an investigation on nanoparticles of spherical shape and studied about the size effect on the thermal performance. The microchannel heat sink consisted of microchannels of trapezoidal shape. This implies that the fluid has more effect on thermal performance as compared to the nanofluids. A detailed review was proposed by Ramezanizadeh [68] on the various approaches for cooling fuel cells. The results of the study show that the use of nanofluids increases the heat transfer and improves the efficiency and also the reduction in size and mass helps in improving the cooling efficiency. Umavathi et al. [69] investigated the mixed convective flow in vertically oriented microchannels which were filled with the electrically conducting viscous fluid. Ramezanizadeh et al. [70] studied the various intelligent methods used for the prediction of thermal conductivity of nanofluids. Abchouyeh [71] studied the heat transfer enhancement using nanofluids between two parallel plates and concluded that with the increase in nanosized particle concentration, the mean Nusselt number increases. The application of nanofluids in thermosyphons was reviewed by Ramezanizadeh et al. [72]. It was explained that the efficiency of thermosyphons increases using nanofluids. Ramezanizadeh et al. [73] investigated nanofluidic thermosyphon heat exchanger using Ni/glycerol–water nanofluid as working fluid in three different concentrations. It was observed that the increase in mass flow rate and inlet temperature of hot stream increases the heat transfer. Chamkha [74] studied the flow of immiscible fluids in porous and non-porous channels in steady laminar regime. It was seen that the increase in the Hartmann number, electrical conductivity ratio and the inverse Darcy number leads to reduction in flow velocities and increases the viscosity ratio. Kumar et al. [75] investigated the fully developed free convective flow in vertical channel using micropolar and viscous fluids. Umavathi et al. [76–79] investigated unsteady two-fluid flow, Couette flow, mixed convection flow and heat and mass transfer in vertically double-passage channel. In the investigation of unsteady two-fluid flow, it was seen that velocity and temperature decrease when the viscosity ratio increases and increase

when the frequency parameter gets increased [76]. It has been seen that the cross-sectional and the structural geometry of microchannel are the most important parameters which affect the flow and heat transfer characteristics. Several studies have been performed by using circular, triangular, trapezoidal, rectangular and square cross sections, and also, researchers have carried out investigations on branched microchannel and fractal-like microchannel heat sink as shown in Fig. 1 [80].

Single-phase flow

Friction factor and pressure drop

Peiyi and Little [81] executed a number of experiments by using gaseous flow instead of liquid flow in microchannels of trapezoidal cross section made of silicon/glass. The experiments were performed to investigate the characteristics of friction factor and pressure drop inside microchannels. Results of their study showed that the flow transition in microchannel occurs very early as compared to the conventional channels. It was observed that the flow transition in microchannels occurs at Reynolds number range of 400–900. It was concluded that the transition also depends upon the test conditions. They made a suggestion to decrease the transition Reynolds number or the critical Reynolds number for microchannels to advance the heat transfer characteristics. Investigation performed by Pfahler et al. [82] used three microchannels having a rectangular cross section. Area of a cross section of these microchannels was in the range of 80–7200 μm^2. In this study, *N*-propanol was used as a flowing fluid. The results of this study interpreted the characteristics of fluid flow and friction factor. Numerous experiments were performed to investigate friction factor in various conditions by using different methods. Peng et al. [83], Wang et al. [84], Peng and Wang [85] and Peng and Peterson [86] concentrated to investigate the fluid flow and heat transfer characteristics for the various structures of microchannels. Yu et al. [87] used nitrogen gas and water as flowing fluid in microchannels having a hydraulic diameter of 19.52 and 102 μm.

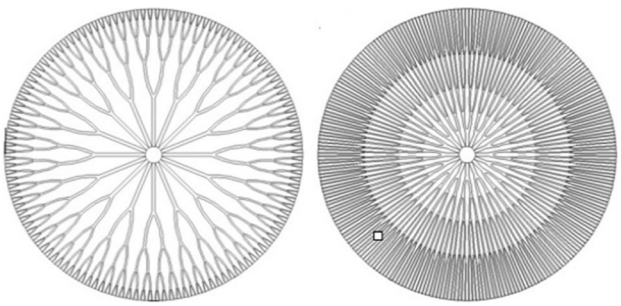

Fig. 1 Fractal-like microchannel network [80]

Hydraulic diameter for a different cross section of channels is defined as,

$$D_h = \frac{A_C}{P_w} \tag{5}$$

where 'A_c' is an area of cross section and 'P_w' is wetted perimeter.

For circular channels, the hydraulic diameter is,

$$D_h = D_i \tag{6}$$

where 'D_i' is the internal diameter of the channel.

For rectangular channels, the hydraulic diameter is,

$$D_h = \frac{4ab}{2(a+b)} \tag{7}$$

where 'a' and 'b' are the sides of the channel.

For Isosceles triangular channel, the hydraulic diameter is,

$$D_h = \frac{a}{2\sqrt{3}} \tag{8}$$

where 'a' is the side of the isosceles triangle.

Researchers have used the classical laminar theory as the basis to understand the nature of fluid flow characteristics in microchannels.

$$C^* = \frac{(f * \mathrm{Re})_{\mathrm{exp}}}{(f * \mathrm{Re})_{\mathrm{theory}}} \tag{9}$$

where 'f' is the friction factor and 'Re' is Reynolds number, but the multiplication of both quantities gives a non-dimensional number. It is calculated experimentally as well as theoretically and the ratio of it gives the 'C^*' as the characteristic quantity. Theoretically, the values of friction factor in circular tubes are calculated as:

For laminar flow:

$$f = \frac{64}{\mathrm{Re}} \tag{10}$$

For turbulent flow:

$$f = 0.3164\mathrm{Re}^{-0.25} \tag{11}$$

A study conducted by Hwang and Kim [88] described the characteristics of pressure drop in the microchannels with internal diameter of 0.244, 0.430 and 0.792 mm, and R134a was used as working fluid to investigate the Reynolds number range of 150–10,000. Yen et al. [89] performed experiment on microchannels having inner diameters of 0.19, 0.30 and 0.51 mm. Flowing fluid used in this study was HCFC123 and FC-72 to observe the variation in heat transfer and fluid flow characteristics. The results of the study showed that when the flow is in the laminar region on the Reynolds number value in the range

of 20–265, then the value of friction factor in microchannels was in agreement with theoretical laminar flow. Celata et al. [90] performed an investigation on microchannel using water as flowing fluid. The investigation was performed experimentally as well as analytically in the Reynolds number range of 20–4000, while the hydraulic diameter of the microchannels was considered between 30 and 344 μm (see Table 3).

In laminar flow regime, the Poiseuille number (P_0) is a constant and given by the product of friction factor and Reynolds number.

$$P_0 = f\,\mathrm{Re} \tag{12}$$

Poiseuille number becomes a very important factor for the rectangular channels as it is a function of aspect ratio. Shah and London [91] proposed a correlation to determine the Poiseuille number. This correlation is as follows,

$$f\,\mathrm{Re} = 24\left(1 - 1.3553\alpha + 1.9467\alpha^2 - 1.7012\alpha^3 + 0.9564\alpha^4 - 0.2537\alpha^5\right) \tag{13}$$

The aspect ratio of the channel must be less than 1, and in some cases, it is greater than 1, and the inverse of it will be taken.

Nikuradse [92] also provides a correlation to calculate the value of Poiseuille number in the pure turbulent regime, which is read as:

$$f = \left[3.48 - 1.737\ln\left(e/D\right)\right]^{-2} \tag{14}$$

where 'e' is absolute roughness of the pipe and 'D' denotes the internal diameter of the pipe.

The friction factor can be calculated by using a relation given by Colebrook et al. [93] given as follows:

$$\frac{1}{\sqrt{f}} = 3.48 - 1.737\ln\left\{\left(\frac{e}{D}\right) + \frac{9.35}{\mathrm{Re}\sqrt{f}}\right\} \tag{15}$$

The work of Kandlikar and Steinke [94] determined the friction factor by using two components. These two components were, friction factor taken from the classical theory of fully developed flow and the second component was Hagenbach factor.

$$\Delta P = \frac{2(f\mathrm{Re})\mu VL}{D_\mathrm{h}^2} + \frac{k(x)\rho\bar{V}^2}{2} \tag{16}$$

where $k(x)$ is known as the Hagenbach factor and given by,

$$k(x) = \left(f_\mathrm{app} - f_\mathrm{FD}\right)\frac{4x}{d_\mathrm{h}} \tag{17}$$

In this relation, f_app and f_FD are known as apparent and fully developed friction factors, respectively. The results of the study showed that this correlation only can predict the friction factor in the laminar region, and for the turbulent region, there is a discrepancy. Since this correlation was developed for the fully developed flow in microchannels and because of temperature variation along with the length of the microchannel, the temperature profile was not completely developed. Thus, this correlation shows deviation from the experimental data. For a rectangular cross section, the Hagenbach factor for fully developed flow is:

$$k(\infty) = \left(0.6796 + 1.2197\alpha + 3.3089\alpha^2 - 9.5921\alpha^3 + 8.9089\alpha^4 - 2.9959\alpha^5\right) \tag{18}$$

Kandlikar and Grande [12] also performed an experiment and presented their findings as correlation to calculate the friction factor in the turbulent regime for fully developed flow.

$$f_\mathrm{app} = \left(0.0929 + \frac{1.01612}{\frac{L}{D_\mathrm{h}}}\right)\mathrm{Re}^{*\left(-0.268 - \frac{0.3298}{\frac{L}{D_\mathrm{h}}}\right)} \tag{19}$$

where Re^* is known as laminar equivalent Reynolds number which was proposed by Jones [95], specifically for rectangular channels only as follows:

$$\mathrm{Re}^* = \mathrm{Re}\left\{\frac{2}{3} + \frac{11}{24}\propto(2-\propto)\right\} \tag{20}$$

It is very important to acknowledge that this correlation was only proposed for minichannels. Later it was confirmed by Kumar et al. [96] that it also can be used for microchannels successfully.

In the past few years, researchers have done work in single-phase flow in microchannels. They have quite explored areas of both liquid flow and gaseous flow. The work done is shown in Table 4 for liquid flow and in Table 5 for gaseous flow. Morini et al. [54] worked in turbulent flow and reported that the experimental value of friction factor was less than that of calculated by Blasius correlation for flow in smooth tubes, even after taking account of compressibility effects. When there is a gaseous

Table 3 Laminar flow in circular and non-circular channels with diameter (D) and sides a and b [90]

Cross section	Geometry	Hydraulic diameter	Constant value
Circular	D	D_h	64
Rectangular	$a/b = 0.1$	$2ab/(a + b)$	85.76
	$a/b = 0.2$	$2ab/(a + b)$	76.8
	$a/b = 0.4$	$2ab/(a + b)$	65.28
	$a/b = 0.6$	$2ab/(a + b)$	60.16
	$a/b = 0.8$	$2ab/(a + b)$	57.6
Square	a	a	56.96

Table 4 Single-phase pressure drop for liquid flow

Author	Year	Flowing fluid	Cross-sectional shape	Hydraulic diameter (D_h)	Reynolds number (Re)	L/D_h	Aspect ratio (w/h)
Tuckerman and Pease [1]	1981	Water	Rectangular	92–96 μm	291–638	104–109	0.17–0.19
Harley et al. [97]	1989	Isopropanol, fluorocarbon	Rectangular, trapezoidal	49.75–66.67 μm	25–250	–	0.5–3.1
Missaggia et al. [98]	1989	Water	Rectangular	160 μm	2350	6	0.25
Pfahler et al. [99]	1990	Isopropanol, silicone oil	Rectangular, trapezoidal	1.6–65 μm	0.0001–300	–	0.008–0.4
Riddle [100]	1991	Water	Rectangular	86–96 μm	96–982	156–180	0.06–0.16
Rahman and Gui [101]	1993	Water	Rectangular	299–491 μm	275–3234	94–154	3.00–6.00
Rahman and Gui [102]	1993	Water and R11	Rectangular	299–491 μm	275–3234	94–154	3.00–6.00
Urbanek et al. [103]	1993	Isopropanol	Trapezoidal, triangular	5–25 μm	–	–	–
Gui and Scaringe [104]	1993	Water	Trapezoidal	338–388 μm	834–9955	119–136	0.73–0.79
Peng et al. [83]	1993	Methanol	Rectangular	311–646 μm	1530–13,455	70–145	0.29–0.86
Wilding et al. [105]	1994	Water and biological fluids	Trapezoidal	26–63 μm	17–126	185.25–438.75	1.0–7.5
Wang and Peng [212]	1994	Water and methanol	Rectangular	311–747 μm	80–3600	60–145	0.29–1.14
Peng and Peterson [106]	1995	Water	Rectangular	311 μm	214–337	145	0.29
Jiang et al. [107]	1995	Water	Rectangular, trapezoidal	20–65 μm	0.006–1.6	39–500	0.11–1.31
Cuta et al. [108]	1995	Water and R124	Rectangular	425 μm	101–578	48	0.27
Cuta et al. [109]	1996	R124	Rectangular	425 μm	101–578	48	0.27
Peng and Peterson [86]	1996	Water	Rectangular	133–200 μm	136–794	25–338	0.5–1.0
Jiang et al. [110]	1997	Water	Circular, trapezoidal	8–68 μm	728	69–276	0.38–0.44
Harms et al. [111]	1997	Water	Rectangular, trapezoidal	404–1923 μm	173–12,900	13–6164	0.04–4.10
Tso and Mahulikar [112]	1998	Water	Circular	728 μm	16.6–37.5	76–89	N/A
Vidmar [113]	1998	Water	Circular	131 μm	2452–7194	580	N/A
Adams et al. [114]	1999	Water	Trapezoidal	131 μm	3899–21,429	141	ID
Mala and Li [115]	1999	Water	Circular	50–254 μm	132–2259	150–490	N/A
Papautsky et al. [116]	1999	Water	Rectangular	44–47 μm	0.002–4	164–177	5.69–26.42

Table 4 (continued)

Author	Year	Flowing fluid	Cross-sectional shape	Hydraulic diameter (D_h)	Reynolds number (Re)	L/D_h	Aspect ratio (w/h)
Meinhart et al. [117]	1999	Water	Rectangular	54.5 μm	–	458.33	0.1
Pfund et al. [118]	2000	Water	Rectangular	253–990 μm	55.3–3501	101–396	19.19–78.13
Qu et al. [119]	2000	Water	Trapezoidal	51–169 μm	6.2–1447	165–543	1.54–14.44
Qu et al. [120]	2000	Water	Trapezoidal	62–169 μm	94–1491	178–482	2.16–11.53
Rahman [121]	2000	Water	Rectangular	299–491 μm	275–3234	94–154	3.00–6.00
Xu et al. [40]	2000	Water	Rectangular	30–344 μm	5–4620	145–1070	0.58–24.53
Ren et al. [122]	2001	Water	Rectangular	28.1–80.3 μm	1–60	10.67–347	124–335
Chung et al. [123]	2002	Water	Circular	100 μm	1.9–3237	875	N/A
Gao et al. [124]	2002	Water	Rectangular	199.2–192 μm	100–8000	42.6–411.6	25–250
Judy et al. [125]	2002	Water, methanol and isopropyl	Circular, rectangular	14–149 μm	7.6–2251	1203–5657	1.00
Lee et al. [126]	2002	Water	Rectangular	85 μm	119–989	118	0.25
Qu and Mudawar [127]	2002	Water	Rectangular	349 μm	137–1670	128	0.32
Celata et al. [128]	2002	R114	Circular	130 μm	100–8000	92	–
Li [129]	2003	Water	Circular	79.9–205.3 μm	300–2500	182–519	–
Bucci et al. [130]	2003	Water	Circular	172–520 μm	2–5272	ID	N/A
Jung and Kwak [131]	2003	Water	Rectangular	100–200 μm	50–325	75–150	1.00–2.00
Lee and Garimella [132]	2003	Water	Rectangular	318–903 μm	558–3636	28–80	0.17–0.22
Park et al. [133]	2003	Water	Rectangular	73 μm	4.2–19.1	654	4.44
Tu and Hrnjak [134]	2003	R134a	Rectangular	69–305 μm	112–3500	131–288	4.11–11.61
Wu and Cheng [135]	2003	Water	Trapezoidal, triangular	26–291 μm	11.1–3060	ID	ID
Wu and Cheng [136]	2003	Water	Trapezoidal	169 μm	16–1378	192–467	1.54–26.20
Baviere et al. [137]	2004	Water	Rectangular	14–593 μm	0.1–7985	138–429	83.33
Hsieh et al. [138]	2004	Water	Rectangular	146 μm	45–969	164	1.74
Lelea et al. [139]	2004	Water	Circular	125.4, 300, 500 μm	50–800	410–857	–
Hao et al. [140]	2005	Water	Trapezoidal	237 μm	50–2800	127	0.361
Steinke et al. [141]	2006	Water	Rectangular	227 μm	14–789	45	0.8
Shen et al. [142]	2006	Water	Rectangular	436 μm	162–1257	16–754	2.67

Table 4 (continued)

Author	Year	Flowing fluid	Cross-sectional shape	Hydraulic diameter (D_h)	Reynolds number (Re)	L/D_h	Aspect ratio (w/h)
Hrnjak and Tu [143]	2007	R134a	Rectangular	69.5–304.7 μm	112–9180	315–691	0.09–0.24
Jung and Kwak [131]	2008	Water	Rectangular	100–200 μm	50–350	75–150	1.00–2.00
Gamrat et al. [144]	2008	Water	Rectangular	100–300 μm	65–2800	107–320	0.33–1.00
Wibel and Ehrhard [145]	2009	Water	Rectangular	127.74–143.9 μm	1200–3000	185.34–208.63	0.23–1.02
Mirmanto et al. [146]	2012	Water	Rectangular	438–635 μm	159–2303	98–142	0.23–0.78
Houshmand and Peles [147]	2013	Nitrogen, water	Circular, rectangular	Circular = 350 μm Rectangular = 383.72	25–2000 (water) 100–6500 (nitrogen)	2.85, 4.54	6.81
do Nascimento et al. [148]	2013	R134a	Rectangular	166.67 μm	–	90	0.2
Balasubramanian et al. [149]	2013	Deionized water	Rectangular (stepped)	480 μm	G = 88–751 kg m^{-2} s^{-1}	4.00	0.25
Goss and Passos [150]	2013	R134a	Circular	0.77 mm	8650–16,300	136.36	–
Liu et al. [50]	2013	R152a	Circular, square	Circular = 1.152 mm Square = 0.952 mm	800–10,100	Circular = 291.67, Square = 335.10	1
Rahimi et al. [151]	2013	Water	Rectangular	0.667 mm	25.99–67.72	329.83	2
Roy et al. [152]	2013	Water	Rectangular	200–54.54 μm	0.00–13.34	1–20	–
Zhuan and Wang [153]	2013	R134a, deionized water	Rectangular	230.76 μm	–	3.33	1.667
El Mghari et al. [154]	2014	Water vapor	Square, rectangular, triangular	250–80 μm	50–210	–	Square = 1 Rectangular = 2, 3, 4, 6, 8, $\propto$ Triangular (Apex angle θ) = 10°–120°
Chen et al. [155]	2014	Deionized water	Rectangular	160 μm and 187.5 μm	350–1500	–	0.25, 0.0667
Emrana and Islama [156]	2014	Water	Rectangular	348.94 μm	225–1450	128.29	0.0245
Huang et al. [157]	2014	Rhodamine B/DI water and Ru(bpy)/dope	Rectangular	102 μm	15–80	392.156	8.77
Law et al. [158]	2014	FC-72	Rectangular	480 μm	–	–	0.25
Leão et al. [159]	2014	R407c	Rectangular	166.67 μm	–	90	0.2

Table 4 (continued)

Author	Year	Flowing fluid	Cross-sectional shape	Hydraulic diameter (D_h)	Reynolds number (Re)	L/D_h	Aspect ratio (w/h)
Nandi et al. [160]	2014	Water	2D wavy	1 (non-dimensional)	0.1–100	–	–
Tan and Liu [161]	2014	Electrolyte solution	Rectangular	16.67 μm	38.58	2999.4	0.5
Abed et al. [162]	2015	Glycerin–water	Square	1.075 mm	50–327	71.63	1
Chandra et al. [163]	2015	Water	Circular (convergent –divergent)	100 μm	50–1000	61.25	–
Dai et al. [164]	2015	Water	Semicircular	2 mm	50–900	–	–
Dehghan et al. [165]	2015	–	Rectangular (width tapered)	333.33 μm	Re < 300	36	0.2
Duryodhan et al. [166]	2015	Deionized water	Trapezoidal (convergent–divergent)	156 μm	30–274	128.205	–
Ebrahimi et al. [167]	2015	Deionized water	Rectangular	1.8 H μm	100–1100	83.33	10
Guo et al. [168]	2015	Water	Regular triangle, regular rectangle, random triangle, random rectangle, 2D Gauss model, 2D fractal model, square column model	500 μm	50–450	40	–
Lee et al. [169]	2015	Deionized water	Rectangular	100 μm and 200 μm	180–680	–	For 100 μm = 3.19–3.37 For 200 μm = 1.97–2.20
Prajapati et al. [170]	2015	Deionized water	Uniform, diverging, segmented	522 μm	50–500	–	0.4 0.533
Rao and Peles [171]	2015	HFE-7000	Rectangular	100–500 μm	–	220	7.1090
Rostami et al. [172]	2015	Water	Square	55–90 μm	50–200	–	1
Vivekanand and Raju [173]	2015	Water	Rectangular	100 μm	–	10	–
Xia et al. [174]	2015	Deionized water	Triangular, trapezoidal, rectangular	0.15 mm	325–650	26.67	0.333
Zhang et al. [175]	2015	Water	Rectangular	129.92 μm 192.42 μm 270.49 μm 312.80 μm	10–600	1539.37, 1039.37, 739.37, 639.374	0.53 1.078 2.696 5.393
Chai et al. [176]	2016	Water	Rectangular, backward triangular, isosceles triangular, forward triangular and semicircular	0.133 mm	190–838	–	0.5
Jagirdar and Lee [177]	2016	Deionized water	Rectangular	0.72 mm	410 − 857	35.28	6.05

Table 4 (continued)

Author	Year	Flowing fluid	Cross-sectional shape	Hydraulic diameter (D_h)	Reynolds number (Re)	L/D_h	Aspect ratio (w/h)
Magnini and Thome [178]	2016	R245fa	Square	0.3–0.7 mm	1000–1500	6	1
Ma et al. [179]	2016	Deionized water	Rectangular	0.15 mm	200–800	33.33	0.33
Prajapati et al. [180]	2016	Deionized water	Rectangular	522 μm	–	49.23	53.33
Sahar et al. [181]	2016	R134a, deionized water	Rectangular	0.561 mm, 0.409 mm	497–4360	7.13, 9.78	0.427
Xu et al. [182]	2016	Water	Rectangular	0.143–0.286 mm	1000–3500	19.79–56.01	0.4–1.332
Yang et al. [183]	2016	HFE-7000, DI water	Rectangular	234.04 μm	106–1152	42.72	0.88
Dalkılıç et al. [184]	2017	R134a	Rectangular	421 μm	3500–6000	95.01	1.23
Feng et al. [185]	2017	Distilled water	Rectangular	0.67 mm	132–1325	–	0.5
Ghani et al. [186]	2017	–	Rectangular	0.2 mm	100–800	25	0.5
Sahar et al. [187]	2017	Water	Rectangular	0.1–1 mm	100–2000	–	1–10
Wan et al. [188]	2017	Deionized water	Rectangular	0.55 mm	<900	81.81	0.83
Zhang et al. [189]	2017	R134a	Square	0.5 mm	–	36	1
Zhou et al. [190]	2018	Deionized water	Rectangular	0.667	50–600	–	0.2
Wang et al. [191]	2018	–	Rectangular	1.67 mm	65–200	42	5
Li et al. [192]	2018	–	Rectangular	80 μm	50–300	–	0.25
Esmailia et al. [193]	2018	Deionized water	Rectangular	133.33 μm	184–1800	150	0.5

Table 5 Single-phase pressure drop for gaseous flow

Author	Year	Channel cross section	Flowing fluid	Hydraulic diameter (D_h)	Reynolds number (Re)	L/D_h	Aspect ratio
Peiyi and little [81]	1983	Rectangular, trapezoidal	Ar, H_2 and N_2	55.8–83.1	100–15,000	100–720	2.37–4.75
Pfahler et al. [99]	1990	Rectangular, trapezoidal	Ar, H_2 and N_2	76.12	0.0009–300	–	0.008–0.4
Choi et al. [194]	1991	Circular	N_2	3.00–81.2	30–20,000	640–8100	0
Pong et al. [195]	1994	Rectangular	N_2 and He	0.03–2.33	–	–	0.03–0.24
Arkilic et al. [196]	1994	Rectangular	He	2.59	0.0014–0.012	2892	39
Yu et al. [87]	1995	Circular	N_2	19–102	250–20,000	<1.00	–
Shih et al. [197]	1996	Rectangular	N_2 and He	2.33	0.001–0.1	1717	33.33
Stanley et al. [198]	1997	Rectangular	N_2	56–256	50–10,000	–	–
Wu et al. [199]	1998	Rectangular	N_2	3.37	0.1–1.00	1305	10.3
Araki et al. [200]	2000	Trapezoidal, triangular	H_2 and N_2	3.92–10.3	0.0065–0.0345	1.59–3.83	1.41–19.71
Turner et al. [201]	2001	Rectangular, trapezoidal	Air, N_2 and He	5–96	0.1–1000	263–5176	20–435
Asako et al. [202]	2005	Circular	N_2	150	1508–2188	206–327	–
Kohl et al. [203]	2005	Rectangular	Air	24.9–99.8	6.8–18,814	220–533	1.03–3.90
Morini et al. [54]	2006	Circular	N_2	133–730	100–10,000	575–3759	–
Tang et al. [204]	2007	Circular Rectangular	N_2	50–300	3–6200	333–3000	–
Morini et al. [205]	2009	Circular	N_2	100–300	100–25,000	167–5000	–
Vijayalakshmi et al. [206]	2009	Trapezoidal	N_2	60.5–211	0.04–0.18	246–860	2.6–3.6
Chen and Zhang [207]	2014	Circular	CO_2	0.1–0.5 mm	3–300	200–800	–
Yuan et al. [208]	2015	Square	Air	0.4 mm	200–2100	243.75	1
Byongjoo Kim [209]	2016	Rectangular	Compressed nitrogen	155–580 μm	30–2500	131.03–490.32	0.25–3.8
Yuan et al. [208]	2016	Circular	Air	0.4 mm	150–2800	25	–

flow, the compressibility effects seem to be more significant as compared to liquid flow. The basic condition for the significance of compressibility effects in gaseous flow occurs when one of these two given conditions as given below are satisfied

$$\mathrm{Ma} > 0.3 \tag{21}$$

$$\frac{\Delta P}{P_{\mathrm{in}}} > 0.05 \tag{22}$$

where 'Ma' denotes the Mach number and 'P_{in}' denotes the pressure drop at inlet of channel.

In the experiment performed by Vijayalakshmi et al. [206], they concluded that pressure distribution is linear in incompressible flow, when the value of Reynolds number exceeds up to 1600. However, pressure distribution linear in nature when the value of Reynolds number goes beyond 1600. These results were in agreement with the results of Kumar et al. [96]. Later on, another experiment performed by Ding et al. [210] explained that, when the value of pressure drop in the duct is nearly 10 kPa, the compressibility effects in gaseous flow tend to be more significant, while the Mach number is kept less than 0.1. Hrnjak and Tu [143] concentrated in the laminar regime and explained that roughness of the channel is not a very significant factor in laminar flow. However, when it comes to turbulent flow, it changes very chaotically and shows its effect on friction factor. Same observations were performed by Tang et al. [204] and stated that roughness factor of microchannels does not play any role in friction factor ergo friction is solely independent of surface roughness in laminar flow. However, the classical theory of fluid flow does not agree with these results. But, many other researchers [12, 87, 90, 118, 119, 210–212] confirmed that the friction factor is closely affected with the change in surface roughness in laminar flow. In some other experiments performed by Morini et al. [54, 205], Kohl et al. [203],

Sharp and Adrian [213] and Hrnjak and Tu [143], they observed that there was no transition reported in laminar to the turbulent regime. According to other studies [81, 83, 86, 104, 115, 210, 212, 214], it was seen that there was an early transition as compared to the classical theory of fluid flow.

Heat transfer

The classical theory of fluid flow defines heat transfer on the basis of Nusselt number, a dimensionless quantity which depends upon heat transfer coefficient, hydraulic diameter of the channel and the thermal conductivity of the fluid flowing in the channel. The value of Nusselt number in fully developed laminar flow regime is 4.364, while the constant heat flux boundary condition was used. Experimental investigation performed by Cuta et al. [108] considered the problem of thermal entrance for laminar flow in combination with constant heat flux. The results of this study observed Nusselt number to be a function of axial distance, Reynolds number and Prandtl number.

$$\mathrm{Nu} = 4.364 + \left\{ \frac{0.00668\left(d_{\mathrm{h}}/x\right)\mathrm{Re}\,\mathrm{Pr}}{1 + 0.04\left[\left(d_{\mathrm{h}}/x\right)\mathrm{Re}\,\mathrm{Pr}\right]^{\frac{2}{3}}} \right\} \tag{23}$$

An experiment was performed by Schilder et al. [215] on single-phase flow while keeping the diameter of the microchannel as 0.6 mm. In another experiment conducted by Admas et al. [114], they worked on the turbulent flow by considering water as flowing fluid in microchannels of circular cross section having hydraulic diameters of 0.76 and 0.109 mm. They proposed a correlation as given below:

$$\mathrm{Nu} = \mathrm{Nu}_{\mathrm{Gn}} + (1 + F) \tag{24}$$

where

$$\mathrm{Nu}_{\mathrm{Gn}} = \frac{\left(\frac{f}{8}\right)(\mathrm{Re} - 1000)\,\mathrm{Pr}}{1 + 12.7\left(\frac{f}{8}\right)^{\frac{1}{2}}\left(\mathrm{Pr}^{\frac{2}{3}} - 1\right)} \tag{25}$$

where 'f' is

$$f = \{1.82\log(\mathrm{Re}) - 1.64\}^{-2} \tag{26}$$

$$F = 7.6 \times 10^{-5}\mathrm{Re}\left\{1 - \left(\frac{d_{\mathrm{h}}}{d_{\mathrm{o}}}\right)^{2}\right\} \tag{27}$$

$\mathrm{Nu}_{\mathrm{Gn}}$ was known as Nusselt number given by Gnielinski [216] in his correlation. Garimella and Singhal [217] proposed both laminar and turbulent conditions and explained that there is a small agreement between experimental results and classical theory. The study concluded that transition from laminar flow to turbulent flow occurs at a very low value of Reynolds number. Mala and Li [115] stated that microchannel flow ceases early transition at low Reynolds number range of 300–900. Peng et al. [83] found the transition to be at 700. Silvério and Moreira [218] contradicted the previous results and stated that the transition does not take place at Reynolds number value less than 1800. These results were in agreement with the results of Sharp and Adrian [213]. Single-phase flow heat transfer is shown in Table 6.

Che et al. [230] investigated Peclet number effect for liquid–liquid two-phase flow heat transfer for rectangular cross-sectional microchannel. The range of Peclet number was kept from 25 to 800. It was observed that with the increase in Peclet number, Nusselt number increases with respect to time as shown in Fig. 2 and decreases the heat transfer index as shown in Fig. 3.

Fischer et al. [231] carried out investigation on laminar heat transfer with water–5 cS silicone oil or PAO as flowing fluids. The nanoparticles of Al_2O_3 having the volume fraction of 3% were suspended in water/PAO droplets. In Fig. 4, the average Nusselt number was compared with non-dimensional pressure drop, normalized by pressure drop of single phase of water flow. Figure 5 shows that the 5 cS silicone oil shows good performance in comparison with other fluid. It was also seen that the addition of nanoparticles into PAO oil enhances the heat transfer and reduces the pressure drop slightly. Figure 5 shows that the highly viscous silicone oil had the highest value of Nusselt number, but the pressure increases about 11% for single-phase fluid flow.

Peiyi and Little [81] performed heat transfer characteristics analysis for both laminar flow and turbulent flow and concluded that values of Nusselt number were greater than as compared to the conventional theory. Later Choi et al. [194] confirmed that correlations given by Peiyi and Little were not in agreement with their experimental results. Extensive study of heat transfer characteristics in single-phase flow in microchannels suggested the following important points:

i. A study performed by [83, 85, 86, 106, 119, 124, 214, 229] concluded that Nusselt number values obtained by experimental results are much less as compared to the conventional theories.
ii. The experimental results of [12, 81, 107, 109, 110, 114, 121, 130, 140, 232–234] confirmed that Nusselt number values are greater as compared to the predicted values of conventional theories.
iii. The results of a study performed by [16, 111, 127, 135, 235, 236] concluded that conventional theories and experimental results are in very good agreement with each other in correlations given for laminar and turbulent flow regimes.

Table 6 Single-phase flow heat transfer

Author	Nature of flow	Channel cross section	Boundary condition	Correlation
Kays [219]	Fully developed	Rectangular	$Re < 2200$	$Nu_{fd} = 8.235\left[1 - \frac{1.883}{\alpha} + \frac{3.767}{\alpha^2} - \frac{5.814}{\alpha^3} + \frac{5.361}{\alpha^4} - \frac{2}{\alpha^5}\right]$
Incropera et al. [220]	Simultaneously developing	Circular	$Re < 2200$	$Nu = 1.86\left(\frac{Re\ Pr\ D}{L}\right)^{\frac{1}{3}}\left(\frac{\mu_f}{\mu_w}\right)^{0.14}$
Incropera et al. [220]	Thermally developing laminar (constant wall temperature)	Circular	$Re < 2200$	$Nu = 3.66 + \frac{0.19\left(\frac{Re\ Pr\ D}{L}\right)^{0.8}}{1+0.117\left(\frac{Re\ Pr\ D}{L}\right)^{0.467}}$
Incropera et al. [220]	Fully developed turbulent	Circular	$Re > 10{,}000$	$Nu = 0.023Re^{0.8}\ Pr^{\frac{1}{3}}$
Incropera et al. [220]	Fully developed turbulent	Circular	$Re > 10{,}000$	$Nu = \frac{\left(\frac{f}{8}\right)Re\ Pr}{K+12.7\left(\frac{f}{8}\right)^{0.5}\left(Pr^{\frac{2}{3}}-1\right)}$
Stephan and Preußer [221]	Simultaneously developing (constant wall temperature)	Circular	$0.7 < Pr < 7$ or $RePrD/L < 33$ for $Pr > 7$	$Nu = 3.657 + \frac{0.0677\left(\frac{Re\ Pr\ D}{L}\right)^{1.33}}{1+0.1\,Pr\left(\frac{ReD}{L}\right)^{0.3}}$
Stephan and Preußer [221]	Simultaneously developing (constant wall temperature)	Circular	$0.7 < Pr < 7$ or $RePrD/L < 33$ for $Pr > 7$	$Nu = 3.657 + \frac{0.0677\left(\frac{Re\ Pr\ D}{L}\right)^{1.33}}{1+0.1\,Pr\left(\frac{ReD}{L}\right)^{0.3}}$
Shah and London [222]	Thermally developing laminar (constant wall heat flux)	Circular	$Re < 2200$	$Nu = \begin{cases} 1.953\left(\frac{Re\ Pr\ D}{L}\right)^{\frac{1}{3}} : \left(\frac{Re\ Pr\ D}{L}\right) \geq 33.3 \\ 4.364 + \frac{0.0722Re\ Pr D}{L} : \left(\frac{Re\ Pr\ D}{L}\right) < 33.3 \end{cases}$
Shah and London [222]	Fully developed laminar	Circular	$Re < 2200$	$Nu = 4.861\left(1 - 3.656\alpha + 12.821\alpha^2 - 27.441\alpha^3 + 37.373\alpha^4 - 28.365\alpha^5 + 8.888\alpha^6\right)$
Kakaç et al. [223]	Transitional	Circular	$2200 < Re < 10{,}000$	$Nu = 0.116\left(Re^{\frac{2}{3}} - 125\right)^{\frac{1}{3}}\left[1 + \left(\frac{D}{L}\right)^{\frac{2}{3}}\right]\left(\frac{\mu_f}{\mu_w}\right)^{0.14}$
Gnielinski [216]	Transitional and fully developed turbulent	Circular	$3000 < Re < 5\ 106$	$Nu = \frac{\langle f/8\rangle(Re-1000)\,Pr}{1+12.7\left(\frac{f}{8}\right)^{0.5}\left(Pr^{\frac{2}{3}}-1\right)} : f = \frac{1}{\{1.82\ln(Re)-1.64\}^2}$
Peiyi and Little [81]	Laminar flow	Rectangular	$Re > 3000$	$Nu = 0.00222Re^{1.09}\ Pr^{0.4}$
Choi et al. [194]	Laminar flow	Rectangular	$Re < 2200$	$Nu = 0.000972Re^{1.17}\ Pr^{1/3}$
Choi et al. [194]	Turbulent flow	Rectangular	$2500 < Re < 20{,}000$	$Nu = 3.82 \times 10^{-6}Re^{1.96}\ Pr^{\frac{1}{3}}$
Yu et al. [224]	Turbulent flow	Rectangular	$6000 < Re < 20{,}000$	$Nu = 0.007Re^{1.2}\ Pr^{0.2}$
Peng et al. [83]	Laminar flow	Rectangular	$Re < 2200$	$Nu = 0.1165\left(\frac{D}{P}\right)^{0.81}\left(\frac{b}{w}\right)^{-0.79}Re^{0.62}\ Pr^{0.33}$
Peng et al. [83]	Turbulent flow	Rectangular	$Re > 10{,}000$	$Nu = 0.072\left(\frac{D}{P}\right)^{1.15}[1 - 2.421(z-0.5)2]Re^{0.8}\ Pr^{0.33}$
Grigull and Tratz [225]	Laminar flow with constant heat flux	Circular	$Re < 2200$	$Nu = 4.36 + \frac{0.00668\left(\frac{d_h}{x}\right)Re\ Pr}{1+0.04\left[\left(\frac{d_h}{x}\right)Re\ Pr\right]^{\frac{2}{3}}}$

Table 6 (continued)

Author	Nature of flow	Channel cross section	Boundary condition	Correlation
Admas et al. [114]	Turbulent flow	Circular	Re > 10,000	$\mathrm{Nu} = \mathrm{Nu}_{\mathrm{Gn}} + (1 + F)$; $\mathrm{Nu}_{\mathrm{Gn}} = \frac{(f/8)(\mathrm{Re}-1000)\,\mathrm{Pr}}{1+12.7\left(\frac{f}{8}\right)^{0.5}\left(\mathrm{Pr}^{\frac{2}{3}}-1\right)}$ $f = \{1.821\log(\mathrm{Re}) - 1.64\}^{-2}$; $F = 7.6 \times 10^{-5}\mathrm{Re}\left\{1 - \left(\frac{d_h}{d_0}\right)^2\right\}$
Bejan [226]	Thermally and hydrodynamically developing laminar flow	ID	Re < 2200	$\mathrm{Nu} = C'\left(\frac{\frac{L}{d_h}}{\mathrm{Re}\,\mathrm{Pr}}\right)^{-0.5}$
Şen and Darici [227]	hydrodynamically developed and thermally developing laminar flow	Circular	Knudsen number = 0.00–0.1	$\mathrm{Nu} = \frac{2q''_{\mathrm{wi}}}{T''_{\mathrm{wi}}-T'_{\mathrm{b}}}$
Fayyadh et al. [228]	Fully developed flow	Rectangular	D_h = 420 mm mass flux range 50–300 kg m^{-2} s	$\mathrm{Nu} = 4.364 + \frac{0.086\left(\mathrm{Re}\,\mathrm{Pr}D_h/L\right)^{1.33}}{1+0.1\left(\mathrm{Re}D_h/L\right)^{0.83}}$ $\mathrm{Nu} = \begin{cases} 1.953\left(\mathrm{Re}\,\mathrm{Pr}\,D_h/L\right)^{1/3}\left(\frac{\mathrm{Re}\,\mathrm{Pr}\,D_h}{L}\right) \geq 33.3 \\ 4.364 + 0.0722\left(\frac{\mathrm{Re}\,\mathrm{Pr}\,D_h}{L}\right)\left(\frac{\mathrm{Re}\,\mathrm{Pr}\,D_h}{L}\right) \geq 33.3 \end{cases}$

It is observed that even though researchers have done extensive studies on microchannels, there are still some deviations in results. Finally, it was concluded that these deviations could be because of the following reasons:

i. Velocity profile and the entrance region are the most crucial area in microchannel flow. Since velocity profile, temperature and the entrance region are in developing mode, the changes in Nusselt number along with the microchannels take place.
ii. The theory of fluid dynamics describes that there are two entrance length: hydrodynamic entrance length and thermal entrance length. When the velocity profile becomes fully developed, then it is necessary to take into account the effects of thermal entrance length.
iii. The complications arise when the value of the Prandtl number becomes greater than unity. In that case, Graetz number becomes the criteria to avoid the entrance effects. Morini [237] suggested taking account the effects of entrance length after Graetz number higher than 10, and Rosa et al. [238] reported that entrance effects might be important at high Reynolds number values.
iv. The difference between inlet and outlet temperatures could be very high in microchannels. Thus, it is possible that the deviation in Nusselt number takes place because of changes in thermophysical properties.

Multi-phase flow

Multi-phase flow is in which the flow takes place in two or more than forms of state of the matter. When two fluids flow in the channels, it is allowed to change its phase in order to provide maximum heat transfer similar to a case of evaporator and condenser. Most common multi-phase flow exists in the form of two-phase flow. Other types of two-phase flows are as follows: liquid–liquid, liquid–gas and gas–gas flows.

Friction factor and pressure drop

In two-phase flow, the flows are classified into two major categories: (1) homogeneous flow and (2) separated flow. In gas–liquid flow, most of the flows are homogeneous flow and suppose to mix up; thus, the calculation of pressure drop can be done by using standard pressured drop correlations. Since only latent heat is assumed to be exchanged between fluids during phase change, the mean properties are computed as weighted as compared to the vapor and liquid percentage present. A number of

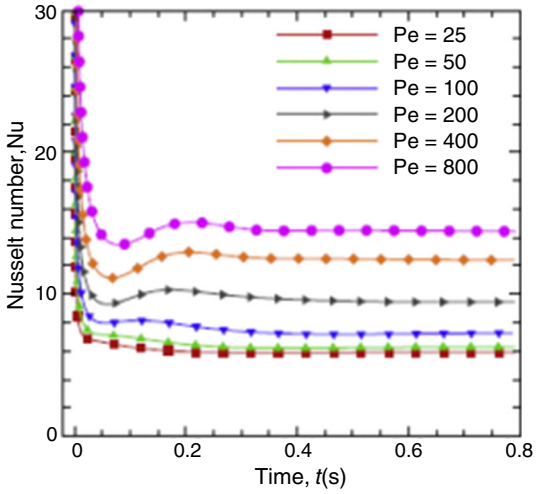

Fig. 2 Nusselt number using varied Peclet numbers with fixed droplet length and the aspect ratio [230]

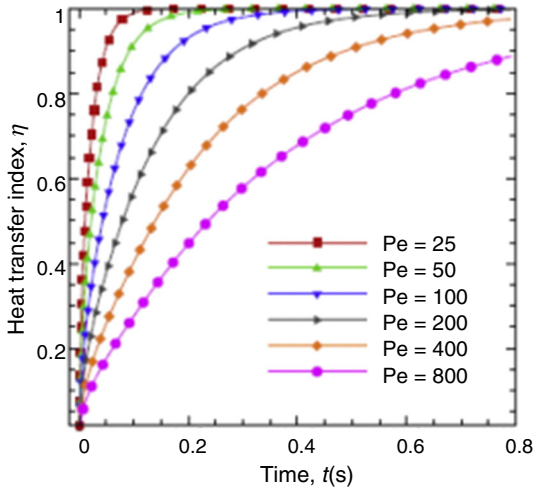

Fig. 3 Heat transfer index using varied Peclet numbers with fixed droplet length and the aspect ratio [230]

correlations for two-phase flow have been suggested. Thoughtful selection of correlation is very important while applying on a model for precise results. Two-phase pressure drop is a function of friction factor, acceleration factor and gravitational factor terms.

$$\frac{dP}{dZ_{\text{total pressure drop}}} = \frac{dP}{dZ_{\text{frictional}}} + \frac{dP}{dZ_{\text{accelaration}}} + \frac{dP}{dZ_{\text{gravitational}}} \tag{28}$$

$$\text{Horizontal flow}: \frac{dP}{dZ_{\text{gravitational}}} = 0 \tag{29}$$

$$\text{Adiabatic flow}: \frac{dP}{dZ_{\text{accelaration}}} = 0 \tag{30}$$

Thus, the total pressure drop,

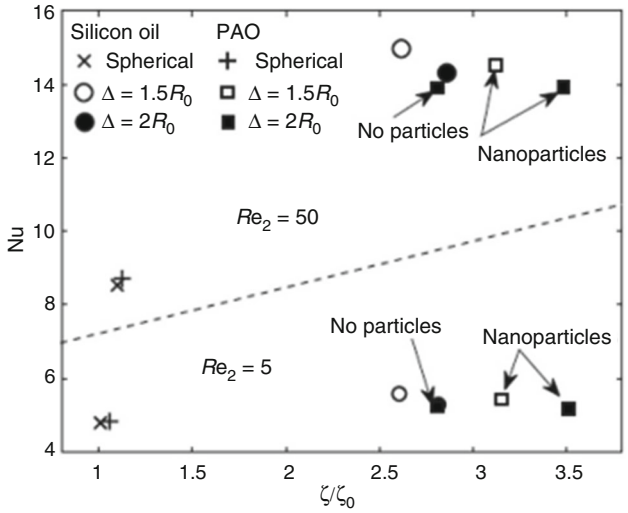

Fig. 4 Averaged Nusselt number versus pressure drop normalized by the pressure drop for differently shaped droplets, with and without nanoparticles [231]

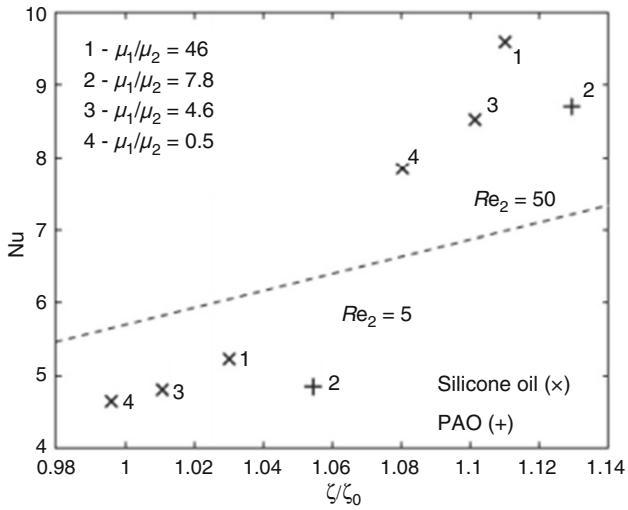

Fig. 5 Averaged Nusselt number versus pressure drop normalized by the pressure drop for spherical droplets with different viscosity ratios [231]

$$\frac{dP}{dZ_{\text{total pressure drop}}} = \frac{dP}{dZ_{\text{frictional}}} = \frac{2f_{\text{TP}}LG^2}{\rho_{\text{TP}}D_{\text{h}}} \tag{31}$$

where 'f_{TP}' is denoted as two-phase friction factor and 'G' is known as mass velocity and is equivalent to $G = \rho v$. Also, ρ_{TP} is known as two-phase density.

$$\rho_{\text{TP}} = \left[\frac{x}{\rho_{\text{G}}} + \frac{1-x}{\rho_{\text{L}}}\right]^{-1} \tag{32}$$

The two-phase friction factor is described as,

- For laminar flow,

$$f_{TP} = \frac{16}{Re_{TP}} \tag{33}$$

- For turbulent flow,

$$f_{TP} = 0.079 Re_{TP}^{-0.25} \tag{34}$$

where two-phase Reynolds number is defined as,

$$Re_{TP} = \frac{GD_h}{\mu_{TP}} \tag{35}$$

where μ_{TP} is known as two-phase viscosity.

The study carried out by Cioncolini et al. [211] introduced a new correlation, which was based on the Weber number. This method of observation at macroscale was also meant to sum up the criteria of microscale in both laminar flows. Another correlation given by Costa-Patry et al. [239] performed an experiment on flow boiling in multi-microchannels having a width of 85 μm. It was concluded that correlation given by Cioncolini was in agreement with their results.

$$f_{TP} = 0.0196\, We_c^{-0.0722} Re_L^{0.318} \tag{36}$$

Few other viscosity models applicable in two phases are as follows:

i. The model is given by McAdams et al. [240]:

$$\mu_{TP} = \left[\frac{x}{\mu_G} + \frac{1-x}{\mu_L}\right]^{-1} \tag{37}$$

ii. The model is given by Owens [241]:

$$\mu_{TP} = \mu_L \tag{38}$$

iii. The model is given by Cicchitti et al. [242]:

$$\mu_{TP} = x\mu_G + (1-x)\mu_L \tag{39}$$

iv. The model is given by Dukler et al. [243]:

$$\mu_{TP} = \beta\mu_G + (1-\beta)\mu_L \tag{40}$$

v. The model is given by Beattie and Whalley [244]:

$$\mu_{TP} = \beta\mu_G + (1-\beta)(1+2.5\beta)\mu_L \tag{41}$$

vi. The model is given by Awad and Muzychka [245]:

$$\mu_{TP} = \frac{2\mu_G + \mu_L - 2(\mu_G - \mu_L)(1-x)}{2\mu_G + \mu_L + (\mu_G - \mu_L)(1-x)} \tag{42}$$

Venkatesan et al. [246], Cioncolini et al. [218] and Choi and Kim [247] identified the two-phase flow patterns and reported that only in case of bubble flow, HFM is applicable in which flow field is with weak disturbance. Liu et al. [248] reported that bubble flow patterns only occur in high flow velocities of liquids and low velocities of gases. However, Taylor flow is also known as slug flow which also demonstrated the applicability of the HFM assumption. Defined criteria for HFM assumption is to where the tube diameter is less than the diameter of bubble length moving along the capillary. In general, slug flow is not always considered as SFM (separated flow model) because flow patterns do not always come into the picture in SFM. Study on two-phase pressure drop is also represented (see Table 7).

Experiment performed by Choi and Kim [247] described one of the most precise viscosity models, a model of Beattie and Whalley. It is focused on volumetric specification. The results reported that Dukler's model over-calculates the two-phase pressure drop, but it is under-calculated by rest of the models. Chung et al. [256] reported that when Dukler's model is used for diameter range of 530–250 μm, it estimates pressure drops. However, when it calculates data in diameter range of 100–50 μm, it shows a good agreement. In another case, it was seen that Beattie and Whalley model was used for the diameter range of 530–250 μm, and it estimates pressure drop very significantly as compared to diameter range of 100–50 μm. Study performed by Choi and Kim at microchannel diameter for D_h = 490 μm reported that Duckler's model is not very precise, but at diameter D_h = 141 μm it predicts pressure drop more precisely. It was also seen that these results was in agreement with the results of Chung et al. [256], while the model of Beattie and Whalley does not show significant difference for microchannel diameters 490 μm and 141 μm.

Figures 6 and 7 show the pressure drop comparison based on the experimental results of two homogenous flow void fraction models (McAdams and Cicchitti) for flow in fractal-like microchannels. The models are in agreement with the experimental results, and the mean deviations for both models are 12.0% and 12.1% and maximum deviation of 20.3% and 20.8% for McAdams and Cicchitti models, respectively. It was stated that both models can overpredict the measured pressure drop values.

A study conducted by Lee and Mudawar [257] explained the two-phase viscosity model predicted by Cicchitti. They explained that this model was slightly different from the rest of the models and provides a greater estimation of two-phase viscosity at very low quality as compared to rest of the models. They described further that the tendency of overprediction of data at low quality and under-prediction of data at higher quality by Cicchitti method gives reasonable mean deviation. This was also verified by the results of Cioncolini et al. [211], Yue et al. [254] and Kawahara et al. [263]. It is important to understand that the best model calculates the pressure drop in two phases which are different for each and every study. It is also important to notice that the hydraulic diameter of characteristics of the two-phase flowing fluid is the key

Table 7 Two-phase pressure drop

Authors	Year	Flowing fluid	Channel cross-sectional geometry	Hydraulic diameter range (D_h)	Reynolds number range (Re)	Developed correlation
Mishima and Hibiki [249]	1996	Water and air	C	1000–4000	–	$C = 21(1 - e^{-0.319D_h})$
Zhang and Webb [250]	2001	R134a R-22 R404a	Circular	2.13 mm	–	When x = 0 (liquid flow); Two-phase multiplier, $\emptyset_{LO}^2 = 1$ When x = 1 (vapor flow); Two-phase multiplier $\emptyset_{LO}^2 = \frac{\left(\frac{dp_{f,vo}}{dz}\right)}{\left(\frac{dp_{f,vo}}{dz}\right)} = \left(\frac{\rho_l}{\rho_v}\right)\left(\frac{f_{vo}}{f_{lo}}\right)$
Lee and Lee [251]	2001	Water and air	R	780–6670	0.303–17,700	$C = A\left(\frac{\mu_L^2}{\rho_L \sigma D_h}\right)^q \left(\frac{\mu_L j}{\sigma}\right) \mathrm{Re}_{LO}^s$
Chen [252]	2002	Water and N_2	C	100	250–20,000	–
Qu and Mudawar [253]	2003	Water	R	349	–	$C = 21(1 - e^{-0.319D_h}) \times (0.00418G + 0.0613)$
Yue et al. [254]	2004	Water and N_2	T	333–528	10–1000	$C = aX^b \mathrm{Re}_{LO}^c$ $a = 0.411822$ $b = -0.0305$ $c = 0.600428$
Coleman and Krause [255]	2004	R134a	R	830	400–40,000	–
Chung et al. [256]	2004	Water N_2	R	50–100	0.0014–0.012	$\frac{dP}{dz}_{F/B} = f_B \frac{\rho_G (U_B - U_l)}{2D_B}$
Lee and Mudawar [257]	2005	R134a	R	349	–	$C = 2.16\mathrm{Re}_{fo}^{0.047}\mathrm{We}_{fo}^{0.6} : L - L$ $C = 1.45\mathrm{Re}_{fo}^{0.25}\mathrm{We}_{fo}^{0.23} : L - T$
Pamitran et al. [258]	2008	CO_2 and R–22	C	1500–3000	–	$C = 1.2897\mathrm{Re}_{tp}^{0.5674}\mathrm{We}_{tp}^{-3.3271}$
Yue et al. [259]	2008	CO_2 and water	C	200–667	0.4–2300	$\emptyset_L^2 = 0.217\beta_L^{-0.5}\mathrm{Re}_{LS}^{0.33}$
Lee and Garimella [260]	2008	Water	R	160–538	–	$C = 2566G^{0.5466}D_h^{0.8819}(1 - e^{-0.319D_h})$
Choi et al. [261]	2008	R410a	Circular	1.5 mm, 3.0 mm	10,000–100,000	$\emptyset_{fo}^2 = \frac{\left(-\frac{dp_F}{dz}\right)_{tp}}{\left(-\frac{dp_F}{dz}\right)_{fo}} = \frac{\left(-\frac{dp_F}{dz}\right)_{tp}}{\frac{2f_{fo}G^2}{D_{pf}}}$
Li and Hibiki [262]	2008	R123, R134a, R22, R236ea, R245fa, R404a, R407c, R410a, R507, CO_2, water and air	–	0.50–12 mm	10–37,000 [liquid] 3–4 × 10^5 [gas]	$C = 1.79\left(\frac{\mathrm{Re}_g}{\mathrm{Re}_l}\right)^{0.4}\left(\frac{1-x}{x}\right)^{0.5}$
Kawahara et al. [263]	2009	Water and ethanol	C	250–500	–	$C = 1.38\mathrm{Bo}^{0.5466}\mathrm{Re}_L^{0.52}\mathrm{We}_G^{-0.12}$: without contraction $C = 0.55\mathrm{Bo}^{0.5466}\mathrm{Re}_L^{0.52}\mathrm{We}_G^{-0.12}$: with contaction
Megahed and Hassan [264]	2009	FC-72	R	70–304	19–4443	$C = \frac{0.0053\mathrm{Re}_{fo}^{0.934}}{\mathrm{Co}^{0.73}(X^2)^{0.175}}$: laminar liquid − laminar vapor $C = \frac{0.0053\mathrm{Re}_{fo}^{1.7}}{\mathrm{Co}^{0.7}(X^2)^{1.24}}$: laminar liquid − laminar vapor

Table 7 (continued)

Authors	Year	Flowing fluid	Channel cross-sectional geometry	Hydraulic diameter range (D_h)	Reynolds number range (Re)	Developed correlation
Choi et al. [194]	2009	Propane	R	1500–3000	–	$C = 1732.953\mathrm{Re}_{tp}^{-0.323}\mathrm{We}_{tp}^{-0.24}$
Lee et al. [265]	2010	Ammonia, CO_2, R11, R12, R22, R123, R134a, R141b, R410a and water	–	0.2–14 mm	0.05×10^3–10.1×10^3 [liquid] 1.2×10^3–155×10^3 [gas]	$C_{new} = 121.6(1 - e^{-22.7Bo})x_e^{1.85}$
Venkatesan et al. [246]	2011	N_2	C	600	–	$C = 4\mathrm{We}_L^{0.3}\left(\frac{\mathrm{Re}_G}{\mathrm{Re}_L}\right)^{0.5}$: $\mathrm{Bo} \geq 1$ $C = 2\mathrm{We}_L^{0.5}\left(\frac{\mathrm{Re}_G}{\mathrm{Re}_L}\right)^{0.5}$: $\mathrm{Bo} < 1$
Garcia et al. [266]	2017	R407c	Circular	4.5 mm, 8 mm	8000–16,000	$\mu_h = \left[\frac{x}{\mu_v} + \frac{(1-x)}{\mu_l}\right]^{-1}$

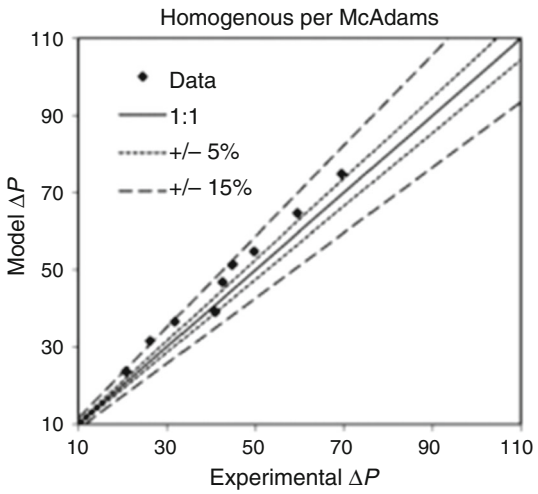

Fig. 6 Homogenous flow models given by McAdams [80]

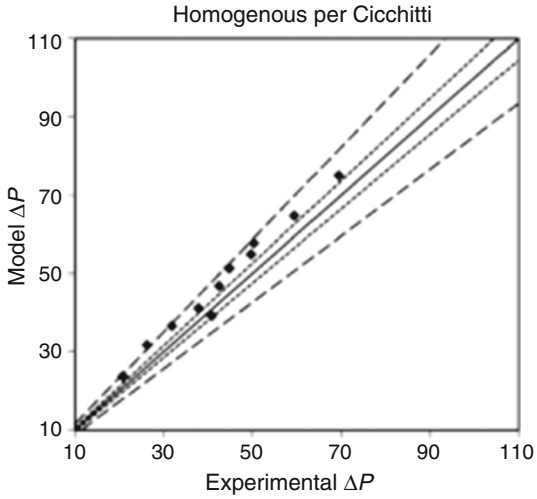

Fig. 7 Homogenous flow models given by Cicchitti [80]

component for the selection of the best model. It was concluded in various studies that the models of Dukler and Cioncolini are capable of predicting the data precisely for microchannels. On the other hand, the models given by Beattie and Whalley and McAdams are best to predict the pressure drop of two phases in minichannels and macrochannels. Separated flow model (SFM) is a model in which both fluids (liquid and gas) flow separately from each other in a channel. Each phase takes up a certain area of the cross section of the channel. Separated flow model has been studied extensively and experiments have been performed as well considering the combination of air–water as flowing fluid. In most of the cases, triangular geometry of cross section of microchannels has been used. Many researchers have performed experiments by considering various hydraulic diameters. Zhao and Bi [267] conducted a study for hydraulic diameters range of 0.87–2.89 mm. Kawahara et al. [263] studied the SFM for nitrogen and

water as flowing fluid in microchannels of circular cross section having a hydraulic diameter of 100 µm. Chung et al. [256] performed experiments on microchannel of square cross section having a hydraulic diameter of 96 µm. A study performed by Lockhart and Martinelli [268] used the concept of the two-phase multiplier for the calculation of pressure drop in liquid flow:

$$\emptyset_{\mathrm{L}}^2 = 1 + \frac{C}{X} + \frac{1}{X^2} \tag{43}$$

$$X = \sqrt{\left[\frac{\left(\frac{\mathrm{d}P}{\mathrm{d}z}\right)_{\mathrm{L}}}{\left(\frac{\mathrm{d}P}{\mathrm{d}z}\right)_{\mathrm{V}}}\right]} \tag{44}$$

The value of two-phase multiplier, denoted by $\emptyset_{\mathrm{L}}^2$ is calculated with the help of coefficient 'C' and a parameter given by Lockhart–Martinelli, X^2, which gives the ratio of single-phase liquid to a single-phase gas pressure gradient. Study conducted by Friedel [269] reported a correlation to calculate the pressure gradient multiplier of two-phase flow as follows:

$$\emptyset_{\mathrm{LO}}^2 = E + \frac{3.24\mathrm{FH}}{\mathrm{Fr}^{0.045}\mathrm{We}^{0.035}} \tag{45}$$

$$E = \left(1 - x^2\right) + x^2 \frac{\rho_{\mathrm{L}} f_{\mathrm{vo}}}{\rho_{\mathrm{v}} f_{\mathrm{Lo}}} \tag{46}$$

where 'Fr' and 'We' are commonly known as Froude and Weber numbers and also f_{vo} and f_{Lo} are known as friction factors of gas and liquid at given mass flux 'G.'

Since many numbers of experimentations were performed below the condition where the value of Reynolds number for gas and liquid ($\mathrm{Re_L}$ and $\mathrm{Re_G}$) was less than 1000, the model of Lockhart and Martinelli estimates the value of 'C' to be 5. The findings of other experiments performed by Yue et al. [254, 259], Chung et al. [256] and Fukano and Kariyasaki [270] depicted that results cannot be well estimated by only one value of 5. Thus, they stated further that the value of C tends to get lower as the diameter of the channel is decreased from 530 to 50 µm. This finding was confirmed by the results of Yue et al. [254], who described that the models given by Lockhart and Martinelli cannot predict dependency of C, well the values of mass flux as good as it does for gas flow and liquid flow on superficial velocities. Many researchers have given other correlations to calculate the value of C_{in} order to further calculate the value of the two-phase multiplier. Experimental results of Cavallini et al. [271] stated that the model is given by Mishima and Hibiki [249] capable of estimating pressure drop in two-phase flow in condensation process of R134a and R-236a in channels having a diameter of 1.4 mm. It was seen that the correlation proposed by Mishima and Hibiki [249] takes account of the dependency of C on the size of the channel, while the channel gap is maintained between 0.4 and 4 mm.

Another equation to estimate the two-phase multiplier was introduced by Chisholm [272] which is as follows:

$$\emptyset_{\mathrm{LO}}^2 = 1 + \left(Y^2 - 1\right)\left[Bx^{2-\frac{\mathrm{n}}{2}}(1-x)^{2-\frac{\mathrm{n}}{2}} + x^{2-\mathrm{n}}\right] \tag{47}$$

where the value of n is 0.25 and Y is known as Chisholm parameter which is as follows:

$$Y = \frac{(\mathrm{d}P/\mathrm{d}Z)_{\mathrm{VO}}}{(\mathrm{d}P/\mathrm{d}Z)_{\mathrm{LO}}} \tag{48}$$

If the value of Chisholm parameter lies between 0 and 9.5, then the value of parameter B is as follows:

$$B = \begin{cases} 4.8 : G \le 500\,\mathrm{kg\,m^{-2}\,s^{-1}} \\ \dfrac{2400}{G} : 500 < G \le 1900\,\mathrm{kg\,m^{-2}} \\ \dfrac{55}{G^{0.5}} : G > 1900\,\mathrm{kg\,m^{-2}\,s^{-1}} \end{cases} \tag{49}$$

When the values of Y lies between 9.5 and 28,

$$B = \begin{cases} \dfrac{520}{YG^{0.3}} : G \le 600\,\mathrm{kg\,m^{-2}\,s^{-1}} \\ \dfrac{21}{Y} : G > 600\,\mathrm{kg\,m^{-2}\,s^{-1}} \end{cases} \tag{50}$$

When $Y \ge 28$,

$$B = \frac{15,000}{Y^2 G^{0.5}} \tag{51}$$

The research was done by Zhang and Webb [250] calculated pressure drop in two-phase flow in adiabatic condition using R404a as flowing fluid in aluminum channel having multi-port extrudes. The hydraulic diameter of the channel was considered as 2.13 mm, and two another tubes made of copper having a hydraulic diameter of 6.25 mm and 3.25 mm were inserted to make it as a concentric channel. Results of this study predicted that correlation given by Friedel cannot estimate two-phase pressure drop precisely. Thus, they proposed a new correlation to calculate the two-phase pressure gradient multiplier as follows:

$$\emptyset_{\mathrm{LO}}^2 = \left(1 - x^2\right) + 2.87x^2\left(\frac{P}{P_{\mathrm{crti}}}\right)^{-1} + 1.68x^{0.8}(1-x)^{0.25}\left(\frac{p}{P_{\mathrm{crit}}}\right)^{-1.64} \tag{52}$$

where critical pressure is denoted by P_{crit} and its value remains constant for each fluid.

An experiment performed by Müller-Steinhagen and Heck [273] used the collection of 9300 measurements values of pressure drop for developing a correlation which is as follows:

$$\left(\frac{dP}{dZ}\right)_f = F(1-x)^{\frac{1}{3}} + \left(\frac{dP}{dZ}\right)_{VO} x^3 \quad (53)$$

where the value of F is given by,

$$F = \left(\frac{dP}{dZ}\right)_{LO} + 2\left[\left(\frac{dP}{dZ}\right)_{VO} - \left(\frac{dP}{dZ}\right)_{LO}\right] x \quad (54)$$

In previous years, when there was a focus on analyzing the flow patterns mainly churn flow and annular flow then it was realized that SFM is very realistic. Some studies [274–276] proposed that little bubble was present in liquid slug flow or the slug–annular flow which is typically not seen in Taylor flow. Basically, churn flow only comes into the picture where high velocity of gaseous flow takes place. It contains big gas bubbles, but slugs are very small as compared to the bubbles. Annular flow occurs at even higher gas flow velocities but for very low velocities of liquids [277]. A study was conducted by Venkatesan et al. [246] to define the naming structure for the flow patterns based on basic characteristics. Slug flow, annular flow and slug–annular flow come under intermittent flow and bubbly flow, and dispersed bubbly flow comes under dispersed flow regime. Some researchers such as Lee and Mudawar [257], Yue et al. [254, 259] and Chung et al. [256] also worked on flow patterns for the analysis of pressure drop in two-phase flow. However, in another experiment performed by Lee and Mudawar [252] concluded that churn flow cannot be very often found by SFM as stated by Yue et al. [254].

Venkatesan et al. [246] experimented on a tube having a diameter of 3.4 mm by considering a model of Dukler with the bubbly regime and reported that only 10% mean deviation from homogeneous flow model (HFM) takes place bubbly flow. Pressure drop was calculated by the mean deviation of 17%. Prediction of slug flow was made by using the correlation given by Chisholm, and the mean deviation was reported to be 14% as compared to the HFM which had the mean deviation of 43%. It was stated that HFM can very well estimate the bubbly flow regime in a tube having a hydraulic diameter of 1.7 mm with the mean deviation of only 7%. On the other hand, for the same diameter, Taylor flow and slug flow were predicted by the mean deviation of 28% and 22%, respectively. The previous results predicted that SFM is reliable to predict the churning flow and slug low. For the prediction of Taylor flow and bubbly flow, HFM is considered best. A study conducted by Venkatesan et al. [246] on annular flow regime reported that when the gas is flowing at high velocities in a tube having a hydraulic diameter of 0.6 mm, annular flow regime cannot be observed, which was in agreement with the results of Chung and Kawaji. It was concluded that it is possible because of strong surface tension force in narrow channels appearing in microchannels which makes the liquid film to incorporate with the gas core comfortably as compared to the minichannels. This is why the existence of annular flow does not take place. Mean deviation between HFMs and experimental results are shown in Table 8.

In two-phase flow in microchannels, viscous forces and inertia forces play a vital role, while the capillary forces are easily negligible [278]. However, it was observed that when the diameter of the tube is reduced then capillary forces comes into the picture and seems to play an important role in the determination of two-phase flow patterns. An experiment performed by Li and Wu [279] described that in theory, there are only four important forces which can be related to the two-phase flow patterns in narrow channels or conventional channels, which are:

(a) Surface tension forces
(b) Gravitational forces
(c) Inertia forces
(d) Viscous forces

The bond number is the term which describes the compression of the dimension of channels and the nominal size of the bubble. It is the actual measure of the available body forces to the surface tension forces in a bubble. Reynolds number holds the significance of the ratio of inertia force to the viscous force, for liquid and gases. On the other side, the ratio of inertia to the surface tension is known as Weber number [118]. It is also notable that viscous force-to-surface tension force ratio is known as a capillary number. Many researchers such as Venkatesan et al. [246], Yue et al. [254, 259], Kawahara et al. [252], Lee and Lee [251], Lee and Mudawar [257], Megahed and Hassan [264], Pamitran et al. [258] and Choi et al. [194] worked on the application of inertia forces and surface tension forces for the estimation of pressure drop in two-phase flow.

Heat transfer

Chen [252] experimented and developed a new correlation to be used in saturated boiling. This correlation is old and precise, and it is compatible very well with the water at low pressure. There are some specific conditions to use this correlation which are as follows:

Hydraulic diameter: $D_h \geq 1$ mm,
Pressure drop range: $P = 0.09$–3.45 MPa
Heat flux range: $q'' = 0$–2.4 MW m^{-2}
Heat transfer coefficient: $h = h_{NB} + h_{FC}$

Forced convection is predicted from the following correlation,

Table 8 Mean deviation between HFM and experimental results

Experiments	Models					
	Mc Adams	Owens	Cicchitti	Dukler	Beattie and Whalley	Lin
Choi and Kim [247], D_h = 490 μm	40.81	352.1	300.7	66.84	30.69	111.99
Choi and Kim [247], D_h = 141 μm	169.87	709.07	650.12	42.1	43.5	346.56
Cioncolini et al. [211]	43.6	40.0	26.6	47.7	39.2	–
Lee and Mudawar [257]	28.26	–	15.98	30.61	26.79	26.44
Yue et al. [254], D_h = 528 μm	19.31	244.38	221.14	–	–	67.54
Yue et al. [254], D_h = 333 μm	18.15	201.92	187.96	–	–	76.91
Kawahara et al. [263], distilled water	28.00	40.5	40.3	33.9	49.0	39.2
Kawahara et al. [263], ethanol 4.8 mass%	59.1	114.9	113.6	27.7	55.2	101.6
Kawahara et al. [263], ethanol 49 mass%	46.6	99.9	99.3	10.4	95.1	90.9
Kawahara et al. [263], ethanol 100 mass%	71.2	110.9	110.1	8.3	93.4	104.5
Average values	52.4	212.62	196.2	33.43	54.11	107.29

$$h_{FC} = 0.023 \mathrm{Re}_f^{0.8} \overset{0.4}{\mathrm{Pr}}_f F(K/d_h) \tag{55}$$

where Re is the Reynolds number and Pr is the Prandtl number:

$$\text{Reynolds number: } \mathrm{Re}_f = \frac{G(1-x)d_h}{\mu_f} \tag{56}$$

$$\text{Prandtl number: } \mathrm{Pr}_f = \left(\frac{\mu C_p}{K}\right)_f \tag{57}$$

'F' is known as the enhancement factor and it was given by Chen [252] and its value is given by $(\mathrm{Re}_{TP}/\mathrm{Re}_f)^{0.8}$.

The phenomenon of nucleate boiling was studied by Forster and Zuber [280], and they developed a correlation to decrease the average value of superheat incorporated with thermal boundary layer and to enhance bubble nucleation phenomenon in cavities that exist in the wall.

$$h_{NB} = 0.00122 \left[\frac{K_f^{0.79} C_{pf}^{0.45} \rho_f^{0.49} g_c^{0.43}}{\sigma^{0.5} \mu_f^{0.29} h_{fg}^{0.24} \rho_g^{0.24}}\right] \Delta T_{sat}^{0.24} \Delta P_{sat}^{0.75} S \tag{58}$$

where

$$\Delta T_{sat} = [T_W - T_{sat}], \text{and } \Delta P_{sat} = [P_{sat}(T_W) - P] \tag{59}$$

In the above equation, 'S' is defined as suppression factor and its value is given by $S = \left[\frac{\Delta T_{eff}}{\Delta T_{sat}}\right]^{0.99}$.

The study conducted by Kandlikar [281] also proposed a correlation to calculate the heat transfer coefficient, which consists of 1000 different data points and all using water, cryogenic fluids and refrigerants as flowing fluids. This can be used only for hydraulic diameter, $D_h \geq 1$ mm.

$$h = \max(h_{NBO}, h_{CBC}) \tag{60}$$

where

$$h_{NBO} = \left[0.6683 \mathrm{Co}^{-0.2} (1-x)^{0.8} f_2(\mathrm{Fr}_{fo}) + 1058 BL^{0.7} (1-x)^{0.8} F_{fL}\right] h_{fo} \tag{61}$$

$$h_{CBC} = \left[1.136 \mathrm{Co}^{-0.9} (1-x)^{0.8} f_2(\mathrm{Fr}_{fo}) + 667.2 \mathrm{BL}^{0.7} (1-x)^{0.8} F_{fL}\right] h_{fo} \tag{62}$$

and

$$h_{fo} = \frac{K_f}{d_h} \frac{(\mathrm{Re}_f - 1000)\left(\frac{f}{2}\right) \mathrm{Pr}_f}{\left[1 + 12.7\left(\mathrm{Pr}_f^{\frac{2}{3}} - 1\right)\left(\frac{f}{2}\right)^{0.5}\right]} \tag{63}$$

In this correlation, 'Co' is called convection number, 'BL' is known as boiling number and 'Fr_{fo}' is called the forced number in the saturated condition of all liquids. The equations used for the above given parameters are given as follows:

$$\mathrm{Co} = (\rho_g/\rho_f)^{0.5} \left[\frac{(1-x)}{x}\right]^{0.8} \tag{64}$$

$$\mathrm{BL} = \frac{q''_w}{G h_{fg}} \tag{65}$$

$$\mathrm{Fr}_{fo} = \frac{G^2}{\rho_f^2 g d_h} \tag{66}$$

Another study conducted by Gungor and Winterton [282] focused on developing a correlation by using 3700 data points by taking ethylene glycol, water and refrigerants as their flowing fluids. The criteria for using the correlation were $d_h \geq 1$ mm. Correlation to calculate the heat transfer coefficient was as follows:

$$h = h_f \left\{ 1 + 3000\mathrm{BL}^{0.86} + 1.12 \left[\frac{1-x}{x} \right]^{0.75} \left(\frac{\rho_g}{\rho_f} \right)^{0.41} \right\} E_2 \tag{67}$$

where the parameter 'E_2' is depended upon the following conditions:

$$E_2 = \begin{cases} 1 : \mathrm{Fr_{fo}} \geq 0.05 \\ \mathrm{Fr_{fo}}^{(1-2\mathrm{Fr_{fo}})} : \mathrm{Fr_{fo}} < 0.05 \end{cases} \tag{68}$$

Few correlations were presented by the study of Shah and London [283]. These correlations were designed to be used for the minichannels and microchannels. They pointed out that both nucleate boiling and convective boiling play a significant role in the study of evaporative heat transfer in two phases. Their correlation was developed to use for both the horizontal and the vertical orientations of tubes. Condition dictates, when $N > 1$ and $\mathrm{BL} > 0.0003$, in that case, the value of heat transfer coefficient (h) is given by the following correlation:

$$h = 230\mathrm{BL}^{0.5} h_f \tag{69}$$

$$N = \left(\frac{1-x}{x} \right)^{0.8} \left(\frac{\rho_g}{\rho_f} \right)^{0.5} \tag{70}$$

However, when $N > 1$ and $\mathrm{BL} < 0.0003$, in this case, the value of heat transfer coefficient (h) is given by,

$$h = \left(1 + 46\mathrm{BL}^{0.5}\right) h_f \tag{71}$$

In another condition, when $0.1 < N < 1$,

$$h = F_s \mathrm{BL}^{0.5} \exp(2.74N - 0.1) h_f \tag{72}$$

And when the value of $N < 0.1$, then 'h' is given by,

$$h = F_s \mathrm{BL}^{0.5} \exp(2.74N - 0.15) h_f \tag{73}$$

where F_s is known as Shah's constant and its value is given by,

Table 9 Two-phase flow heat transfer

Authors	Year	Flowing fluid	Channel geometry
Lazarek and Black [284]	1982	R113	Circular
Cornwell and Kew [285]	1992	R113	Rectangular
Moriyama et al. [286]	1992	R113	Rectangular
Bowers and Mudawar [287]	1993	R113	Minichannels
Wambsganss et al. [288]	1993	R113	Circular
Mertz et al. [289]	1996	Water, R141b	Rectangular
Kew and Cornwell [290]	1997	R141b	Circular
Ravigururajan [234]	1998	R124	Rectangular
Mehendale and Jacobi [291]	2000	R134a	Rectangular
Kawahara et al. [263]	2002	Water, nitrogen	Circular
Lee and Mudawar [257]	2005	R134a	Rectangular
Zhao et al. [292]	2006	Water, kerosene	Rectangular
Hrnjak and Luo [143]	2008	Water, CO_2	Rectangular
Agostini et al. [293]	2008	R236fa	Rectangular
Megahed and Hassan [264]	2009	FC-72	Rectangular
Ergu et al. [294]	2009	Water	Rectangular
Alapati et al. [295]	2009	NA	Rectangular
Na and Chung [296]	2011	ID	Circular
Megahed and Hassan [264]	2012	FC-72	Rectangular
Liu et al. [41]	2012	Methanol, helium	Rectangular
Autee et al. [297]	2012	Water, air	Circular
Ide et al. [298]	2012	Water, nitrogen,	Circular
Costa-Patry et al. [239]	2012	R245fa, R236fa	Rectangular
Szczukiewicz et al. [299]	2013	R236fa, R245fa	Circular
do Nascimento et al. [148]	2013	R134a	Rectangular
Goss and Passos [150]	2013	R134a	Circular
Houshmand and Peles [300]	2014	Air–water	Rectangular
Suwankamnerd and Wongwises [301]	2015	Air–water	Rectangular
Chinnov et al. [302]	2016	Air/nitrogen and water	Rectangular
Vanderputten et al. [303]	2017	R134a	Rectangular
Dalkılıç et al. [304]	2018	R134a	Rectangular

$$F_s = \begin{cases} 15.43 : \mathrm{BL} < 0.0011 \\ 14.7 : \mathrm{BL} > 0.0011 \end{cases} \quad (74)$$

A study conducted by Li and Wu [279] used 3744 data points to develop a correlation with the help of parameters such as Reynolds number, boiling number and bond number. This correlation can be used for many different flowing fluids, on various operating conditions and for different geometries, orientations and dimensions of microchannels. They deduced from their results that bond number is a parameter which can be used to define the criteria for estimating the heat transfer coefficient. It was stated that the correlation can be used only for the condition where 0.19 mm $\leq d_h \leq$ 2.01 mm:

$$h = 334\mathrm{BL}^{0.3}\left(\mathrm{Bo}\,\mathrm{Re}_f^{0.36}\right)^{0.4}\left(\frac{K_f}{d_h}\right) \quad (75)$$

$$\mathrm{Bo} = \frac{g\left(\rho_L - \rho_g\right)d_h^2}{\sigma} \quad (76)$$

A number of experiments have been performed, and the results are published to define the pressure drop and heat transfer characteristics of microchannels. Researchers have worked in both areas—single-phase flow and two-phase flow—and finally, it was concluded that either results were deviating from conventional theory of fluid flow and heat transfer or they simply were not in agreement with others. Two-phase flow heat transfer is shown in Table 9. Heat transfer characteristics of microchannels show much more deviation as compared to the pressure drop. However, in some of the studies, it was seen that results of some researchers were in agreement with the conventional theories, but in few other cases, the results were completely different, while the operating condition, hydraulic diameter and flowing fluid were kept same. Some new correlation was developed in order to predict the friction factor and Nusselt number. Their correlation was developed by using the many numbers of data point collectively, and they were not based on any theoretical assumptions or hypothesis; thus, this correlation cannot be assumed as much reliable and significance.

Conclusions and recommendations for future studies

The present paper presents an extensive review in the area of fluid flow and heat transfer in microchannels for single-phase as well as multi-phase flows. It was observed that single-phase flow in microchannels having a hydraulic diameter of few hundred micrometers, fluid is considered to be incompressible, while the flow becomes fully developed. However, the flow is taking place in laminar flow regime at constant temperature boundary condition seems to follow the classical theory of fluid flow. Various experiments performed at low value ranges of Reynolds number concluded that the experimental results were in agreement with the theoretical prediction. However, it was seen as the value of Reynolds number becomes higher; then, the experimental results start to deviate from the conventional laminar predictions. It was also noted that experimental results seem to follow the conventional thermal developing flow pattern when the hydraulic diameter of the microchannel is increased. On the other side, the experimental results of pressure drop show a slight agreement for both laminar and turbulent regimes. It is possible that the deviations occurred in pressure drop in laminar and turbulent regimes may be because the correlations were developed by assumed macroscale behavior. Researchers only explored the laminar region for its pressure drop and heat transfer characteristics, while the turbulent flow regime is yet to be explored for pressure drop and heat transfer characteristics. So, it is highly recommended to work in this direction.

References

1. Tuckerman DB, Pease RFW. High-performance heat sinking for VLSI. IEEE Electron Device Lett. 1981;2(5):126–9.
2. Phillips RJ. Forced-convection, liquid-cooled, microchannel heat sinks, US4894709A, 09 March 1988.
3. Hahn R, et al. High power multichip modules employing the planar embedding technique and microchannel water heat sinks. IEEE Trans Compon Packag Manuf Technol A. 1997;20(4):432–40.
4. Martin PM, Bennett WD, Johnston JW. Microchannel heat exchangers for advanced climate control. 1995. https://www.spiedigitallibrary.org. Accessed 1 Aug 2019.
5. Vydai AV, Soshelev SB, Reznikov GV, Kharitonov VV, Cheremuskhin SV. Thermophysical design of the parameters of a computer board with a microchannel cooling system. J Eng Phys Thermophys. 1993;64(1):80–6.
6. Beach R, et al. Modular microchannel cooled heatsinks for high average power laser diode arrays. IEEE J Quantum Electron. 1992;28(4):966–76.
7. Mundinger D, et al. Demonstration of high-performance silicon microchannel heat exchangers for laser diode array cooling. Appl Phys Lett. 1988;53(12):1030–2.
8. Missaggia LJ, Walpole JN, Liau ZL, Phillips RJ. Microchannel heat sinks for two-dimensional high-power-density diode laser arrays. IEEE J Quantum Electron. 1989;25(9):1988–92.
9. Bazdar H, Toghraie D, Pourfattah F, Akbari OA, Nguyen HM, Asadi A. Numerical investigation of turbulent flow and heat transfer of nanofluid inside a wavy microchannel with different wavelengths. J Therm Anal Calorim. 2019;135(6):3471–83.
10. Serizawa A, Feng Z, Kawara Z. Two-phase flow in microchannels. Exp Therm Fluid Sci. 2002;26(6–7):703–14.
11. Mehendale SS, Jacobi AM, Shah RK. Fluid flow and heat transfer at micro- and meso-scales with application to heat exchanger design. Appl Mech Rev. 2009;53(7):175.

12. Kandlikar SG, Grande WJ. Evaluation of single phase flow in microchannels for high heat flux chip cooling—thermohydraulic performance enhancement and fabrication technology. Heat Transf Eng. 2004;25(8):5–16.
13. Palm B. Heat transfer in microchannels. Microscale Thermophys Eng. 2001;5(3):155–75.
14. Stephan P. Microscale evaporative heat transfer: modelling and experimental validation. 2019. p. 13. http://ihtcdigitallibrary.com/. Accessed 2 Aug 2019.
15. Halelfadl S, Adham AM, Mohd-Ghazali N, Maré T, Estellé P, Ahmad R. Optimization of thermal performances and pressure drop of rectangular microchannel heat sink using aqueous carbon nanotubes based nanofluid. Appl Therm Eng. 2014;62(2):492–9.
16. Warrier GR, Kim CJ, Ju YS. Microchannel cooling device with perforated side walls: design and modeling. Int J Heat Mass Transf. 2014;68:174–83.
17. Yu XF, et al. A study on the hydraulic and thermal characteristics in fractal tree-like microchannels by numerical and experimental methods. Int J Heat Mass Transf. 2012;55(25–26):7499–507.
18. Wang L, Wu W, Li X. Numerical and experimental investigation of mixing characteristics in the constructal tree-shaped microchannel. Int J Heat Mass Transf. 2013;67:1014–23.
19. Wang XQ, Mujumdar AS, Yap C. Thermal characteristics of tree-shaped microchannel nets for cooling of a rectangular heat sink. Int J Therm Sci. 2006;45(11):1103–12.
20. Senn SM, Poulikakos D. Laminar mixing, heat transfer and pressure drop in tree-like microchannel nets and their application for thermal management in polymer electrolyte fuel cells. J Power Sources. 2004;130(1–2):178–91.
21. Tuo H, Hrnjak P. Effect of venting the periodic reverse vapor flow on the performance of a microchannel evaporator in air-conditioning systems. Int J Heat Mass Transf. 2014;69:66–76.
22. Chamkha AJ, Groşan T, Pop I. Fully developed free convection of a micropolar fluid in a vertical channel. Int Commun Heat Mass Transf. 2002;29(8):1119–27.
23. Chamkha AJ, Grosan T, Pop I. Fully developed mixed convection of a micropolar fluid in a vertical channel. Int J Fluid Mech Res. 2003;30(3):251–63.
24. Chamkha AJ. Hydromagnetic two-phase flow in a channel. Int J Eng Sci. 1995;33(3):437–46.
25. Chamkha AJ. Unsteady laminar hydromagnetic fluid–particle flow and heat transfer in channels and circular pipes. Int J Heat Fluid Flow. 2000;21(6):740–6.
26. Chamkha AJ. Unsteady laminar hydromagnetic flow and heat transfer in porous channels with temperature-dependent properties. Int J Numer Methods Heat Fluid Flow. 2001;11(5–6):430–48.
27. Chamkha AJ. On laminar hydromagnetic mixed convection flow in a vertical channel with symmetric and asymmetric wall heating conditions. Int J Heat Mass Transf. 2002;45(12):2509–25.
28. Chamkha AJ, Molana M, Rahnama A, Ghadami F. On the nanofluids applications in microchannels: a comprehensive review. Powder Technol. 2018;332:287–322.
29. Ibáñez G, López A, López I, Pantoja J, Moreira J, Lastres O. Optimization of MHD nanofluid flow in a vertical microchannel with a porous medium, nonlinear radiation heat flux, slip flow and convective–radiative boundary conditions. J Therm Anal Calorim. 2019;135(6):3401–20.
30. Shashikumar NS, Gireesha BJ, Mahanthesh B, Prasannakumara BC, Chamkha AJ. Entropy generation analysis of magneto-nanoliquids embedded with aluminium and titanium alloy nanoparticles in microchannel with partial slips and convective conditions. Int J Numer Methods Heat Fluid Flow. 2018.
31. Khodabandeh E, Rozati SA, Joshaghani M, Akbari OA, Akbari S, Toghraie D. Thermal performance improvement in water nanofluid/GNP–SDBS in novel design of double-layer microchannel heat sink with sinusoidal cavities and rectangular ribs. J Therm Anal Calorim. 2019;136(3):1333–45.
32. Park CY, Hrnjak P. Experimental and numerical study on microchannel and round-tube condensers in a R410a residential air-conditioning system. Int J Refrig. 2008;31(5):822–31.
33. Qu X, Shi J, Qi Z, Chen J. Experimental study on frosting control of mobile air conditioning system with microchannel evaporator. Appl Therm Eng. 2011;31(14–15):2778–86.
34. Qi Z, Zhao Y, Chen J. Performance enhancement study of mobile air conditioning system using microchannel heat exchangers. Int J Refrig. 2010;33(2):301–12.
35. Tuo H, Hrnjak P. Periodic reverse flow and boiling fluctuations in a microchannel evaporator of an R134a mobile air-conditioning system. SAE Int J Mater Manuf. 2013;6(3):540–8.
36. Jin J, Chen J, Chen Z. Development and validation of a microchannel evaporator model for a CO_2 air-conditioning system. Appl Therm Eng. 2011;31(2–3):137–46.
37. Yun R, Kim Y, Park C. Numerical analysis on a microchannel evaporator designed for CO_2 air-conditioning systems. Appl Therm Eng. 2007;27(8–9):1320–6.
38. Kim M-H, Bullard CW. Development of a microchannel evaporator model for a CO_2 air-conditioning system. Energy. 2001;26(10):931–48.
39. Moallem E, Cremaschi L, Fisher DE, Padhmanabhan S. Experimental measurements of the surface coating and water retention effects on frosting performance of microchannel heat exchangers for heat pump systems. Exp Therm Fluid Sci. 2012;39:176–88.
40. Xu B, et al. Experimental investigation of frost and defrost performance of microchannel heat exchangers for heat pump systems. Appl Energy. 2013;103:180–8.
41. Liu TL, Fu BR, Pan C. Boiling heat transfer of co- and counter-current microchannel heat exchangers with gas heating. Int J Heat Mass Transf. 2013;56(1–2):20–9.
42. Shao LL, Yang L, Zhang CL. Comparison of heat pump performance using fin-and-tube and microchannel heat exchangers under frost conditions. Appl Energy. 2010;87(4):1187–97.
43. Zou Y, Hrnjak PS. Experiment and visualization on R134a upward flow in the vertical header of microchannel heat exchanger and its effect on distribution. Int J Heat Mass Transf. 2013;62(1):124–34.
44. Dasgupta ES, Askar S, Ismail M, Fartaj A, Quaiyum MA. Air cooling by multiport slabs heat exchanger: an experimental approach. Exp Therm Fluid Sci. 2012;42:46–54.
45. Han Y, Liu Y, Li M, Huang J. A review of development of micro-channel heat exchanger applied in air-conditioning system. Energy Procedia. 2012;14:148–53.
46. Garimella S, Determan MD, Meacham JM, Lee S, Ernst TC. Microchannel component technology for system-wide application in ammonia/water absorption heat pumps. Int J Refrig. 2011;34(5):1184–96.
47. Fronk BM, Garimella S. Water-coupled carbon dioxide microchannel gas cooler for heat pump water heaters: part II—model development and validation. Int J Refrig. 2011;34(1):17–28.
48. Park CY, Hrnjak P. Effect of heat conduction through the fins of a microchannel serpentine gas cooler of transcritical CO_2 system. Int J Refrig. 2007;30(3):389–97.
49. Languri EM, Hooman K. Slip flow forced convection in a microchannel with semi-circular cross-section. Int Commun Heat Mass Transf. 2011;38(2):139–43.

50. Liu N, Li JM, Sun J, Wang HS. Heat transfer and pressure drop during condensation of R152a in circular and square microchannels. Exp Therm Fluid Sci. 2013;47:60–7.
51. Hrnjak P, Litch AD. Microchannel heat exchangers for charge minimization in air-cooled ammonia condensers and chillers. Int J Refrig. 2008;31(4):658–68.
52. Pettersen J, Hafner A, Skaugen G, Rekstad H. Development of compact heat exchangers for CO_2 air-conditioning systems. Int J Refrig. 1998;21(3):180–93.
53. Goodman C, Fronk BM, Garimella S. Transcritical carbon dioxide microchannel heat pump water heaters: part I—validated component simulation modules. Int J Refrig. 2011;34(4):859–69.
54. Morini GL, Lorenzini M, Salvigni S, Spiga M. Thermal performance of silicon micro heat-sinks with electrokinetically-driven flows. Int J Therm Sci. 2006;45(10):955–61.
55. Sarangi RK, Bhattacharya A, Prasher RS. Numerical modelling of boiling heat transfer in microchannels. Appl Therm Eng. 2009;29(2–3):300–9.
56. Zhang Q, Tang D, Li D, Peng Y. Numerical and experimental study on in-plane bending of microchannel aluminum flat tube. J Mater Process Technol. 2010;210(14):1876–84.
57. Agarwal A, Bandhauer TM, Garimella S. Measurement and modeling of condensation heat transfer in non-circular microchannels. Int J Refrig. 2010;33(6):1169–79.
58. Al-Hajri E, Shooshtari AH, Dessiatoun S, Ohadi MM. Performance characterization of R134a and R245fa in a high aspect ratio microchannel condenser. Int J Refrig. 2013;36(2):588–600.
59. Vakili-Farahani F, Agostini B, Thome JR. Experimental study on flow boiling heat transfer of multiport tubes with R245fa and R1234ze(E). Int J Refrig. 2013;36(2):335–52.
60. Moallem E, Hong T, Cremaschi L, Fisher DE. Experimental investigation of adverse effect of frost formation on microchannel evaporators, part 1: effect of fin geometry and environmental effects. Int J Refrig. 2013;36(6):1762–75.
61. Thompson SM, Ma HB, Wilson C. Investigation of a flat-plate oscillating heat pipe with Tesla-type check valves. Exp Therm Fluid Sci. 2011;35(7):1265–73.
62. Nielsen KK, Engelbrecht K, Christensen DV, Jensen JB, Smith A, Bahl CRH. Degradation of the performance of microchannel heat exchangers due to flow maldistribution. Appl Therm Eng. 2012;40:236–47.
63. Kim NH, Byun HW, Sim YS. Upward branching of two-phase refrigerant in a parallel flow minichannel heat exchanger. Exp Therm Fluid Sci. 2013;51:189–203.
64. Szczukiewicz S, Borhani N, Thome JR. Fine-resolution two-phase flow heat transfer coefficient measurements of refrigerants in multi-microchannel evaporators. Int J Heat Mass Transf. 2013;67:913–29.
65. Alam T, Lee PS, Yap CR, Jin L. A comparative study of flow boiling heat transfer and pressure drop characteristics in microgap and microchannel heat sink and an evaluation of microgap heat sink for hotspot mitigation. Int J Heat Mass Transf. 2013;58(1–2):335–47.
66. Fani B, Abbassi A, Kalteh M. Effect of nanoparticles size on thermal performance of nanofluid in a trapezoidal microchannel-heat-sink. Int Commun Heat Mass Transf. 2013;45:155–61.
67. Hung TC, Sheu TS, Yan WM. Optimal thermal design of microchannel heat sinks with different geometric configurations. Int Commun Heat Mass Transf. 2012;39(10):1572–7.
68. Ramezanizadeh M, Nazari MA, Ahmadi MH, Chen L. A review on the approaches applied for cooling fuel cells. Int J Heat Mass Transf. 2019;139:517–25.
69. Umavathi JC, Mohiuddin S, Sheremet MA. MHD flow in a vertical channel under the effect of temperature dependent physical parameters. Chin J Phys. 2019;58:324–38.
70. Ramezanizadeh M, Nazari MA, Ahmadi MH, Lorenzini G, Pop I. A review on the applications of intelligence methods in predicting thermal conductivity of nanofluids. J Therm Anal Calorim. 2019;3:1–17.
71. Abchouyeh MA, Fard OS, Mohebbi R, Sheremet MA. Enhancement of heat transfer of nanofluids in the presence of sinusoidal side obstacles between two parallel plates through the lattice Boltzmann method. Int J Mech Sci. 2019;156:159–69.
72. Ramezanizadeh M, Alhuyi Nazari M, Ahmadi MH, Açıkkalp E. Application of nanofluids in thermosyphons: a review. J Mol Liq. 2018;272:395–402.
73. Ramezanizadeh M, Alhuyi Nazari M, Ahmadi MH, Chau KW. Experimental and numerical analysis of a nanofluidic thermosyphon heat exchanger. Eng Appl Comput Fluid Mech. 2019;13(1):40–7.
74. Chamkha AJ. Flow of two-immiscible fluids in porous and nonporous channels. J Fluids Eng. 2002;122(1):117.
75. Kumar JP, Umavathi JC, Chamkha AJ, Pop I. Fully-developed free-convective flow of micropolar and viscous fluids in a vertical channel. Appl Math Model. 2010;34(5):1175–86.
76. Umavathi JC, Chamkha AJ, Mateen A, Al-Mudhaf A. Unsteady two-fluid flow and heat transfer in a horizontal channel. Heat Mass Transf. 2005;42(2):81–90.
77. Umavathi JC, Chamkha AJ, Sridhar KSR. Generalized plain couette flow and heat transfer in a composite channel. Transp Porous Media. 2010;85(1):157–69.
78. Umavathi JC, Sheremet MA, Mohiuddin S. Combined effect of variable viscosity and thermal conductivity on mixed convection flow of a viscous fluid in a vertical channel in the presence of first order chemical reaction. Eur J Mech B/Fluids. 2016;58:98–108.
79. Umavathi JC, Kumar JP, Sheremet MA. Heat and mass transfer in a vertical double passage channel filled with electrically conducting fluid. Phys A Stat Mech Appl. 2017;465:195–216.
80. Daniels BJ, Liburdy JA, Pence DV. Experimental studies of adiabatic flow boiling in fractal-like branching microchannels. Exp Therm Fluid Sci. 2011;35(1):1–10.
81. Peiyi W, Little WA. Measurement of friction factors for the flow of gases in very fine channels used for microminiature Joule–Thomson refrigerators. Cryogenics (Guildf). 1983;23(5):273–7.
82. Pfahler J, Harley J, Bau H, Zemel J. Liquid transport in micron and submicron channels. Sens Actuators A: Phys. 1990;22(1–3):431–4.
83. Peng XF, Wang BX, Peterson GP, Ma HB. Experimental investigation of heat transfer in flat plates with rectangular microchannels. Int J Heat Mass Transf. 1995;38(1):127–37.
84. Wang L, Yang JT, Lyu PC. An overlapping crisscross micromixer. Chem Eng Sci. 2007;62(3):711–20.
85. Peng XF, Wang B-X. Forced convection and flow boiling heat transfer for liquid flowing through microchannels. Int J Heat Mass Transf. 1993;36(14):3421–7.
86. Peng XF, Peterson GP. Convective heat transfer and flow friction for water flow in microchannel structures. Int J Heat Mass Transf. 1996;39(12):2599–608.
87. Yang G, Ebadian MA, Soliman HM. An experimental and theoretical study of laminar fluid flow and heat transfer in helical coils. 2019. pp. 321–326. https://ci.nii.ac.jp/. Accessed 5 Aug 2019.
88. Hwang YW, Kim MS. The pressure drop in microtubes and the correlation development. Int J Heat Mass Transf. 2006;49(11–12):1804–12.
89. Yen T-H, Kasagi N, Suzuki Y. Forced convective boiling heat transfer in microtubes at low mass and heat fluxes. Int J Multiph Flow. 2003;29:1771–92.

90. Celata GP, Cumo M, Mariani A, Nariai H, Inasaka F. Influence of channel diameter on subcooled high heat fluxes. Int J Heat Mass Transf. 1993;36(13):3407–10.
91. Shah RK, London AL. Chapter II—differential equations and boundary conditions. In: Laminar flow forced convect. Ducts. 1978, pp. 5–36.
92. Nikuradse J. Laws of flow in rough pipes, vol. 3, no. November. Washington: National Advisory Committee for Aeronautics. 1950.
93. Colebrook CF, et al. Turbulent flow in pipes, with particular reference to the transition region between the smooth and rough pipe laws. (includes plates). J Inst Civ Eng. 1939;12(8):393–422.
94. Kandlikar SG, Steinke ME. Single-phase liquid friction factors in microchannel. Int J Therm Sci. 2006;45:1073–83.
95. Jones OC. An improvement in the calculation of turbulent friction in rectangular ducts. J Fluids Eng. 1976;98(2):173.
96. Kumar V, Paraschivoiu M, Nigam KDP. Single-phase fluid flow and mixing in microchannels. Chem Eng Sci. 2011;66(7):1329–73.
97. Harley J, Bau H, Zemel JN, Dominko V. Fluid flow in micron and submicron size channels. 2003, pp. 25–28. http://ieeexplore.ieee.org/. Accessed 5 Aug 2019.
98. Missaggia LJ, Walpole JN, Liau ZL, Phillips RJ. Microchannel heat sinks for two-dimensional high-power-density diode laser arrays. Quantum Electron IEEE J. 1989;25(9):1988–92.
99. Pfahler J, Harley J, Bau HH, Zemel J. Liquid and gas transport in small channels. In: Micromechanics and MEMS: classic and seminal papers to 1990. 1997. pp. 478–486.
100. Riddle R. Design calculations for the microchannel heatsink. 1991. http://adsabs.harvard.edu/. Accessed 6 Aug 2019.
101. Rahman MM, Gui F. Experimental measurements of fluid flow and heat transfer in microchannel cooling passages in a chip substrate. In: The ASME international electronics packaging conference. 1993. pp. 685–692.
102. Rahman MM, Gui F. Design, fabrication, and testing of microchannel heat sinks for aircraft avionics cooling. In: Intersociety energy conversion engineering conference. 1993. p. 1.
103. Urbanek W, Zemel JN, Bau HH. An investigation of the temperature dependence of Poiseuille numbers in microchannel flow. J Micromech Microeng. 1993;3(4):206–9.
104. Gui F, Scaringe R. Enhanced heat transfer in the entrance region of microchannels. 1995.
105. Wilding P, Pfahier J, Bau HH, Zemel JN, Krlcka LJ. Manipulation and flow of biological fluids in straight channels micromachined in silicon. 1994. vol. 40, no. 1, pp. 43–47. http://clinchem.aaccjnls.org/. Accessed 7 Aug 2019.
106. Peng XF, Peterson GP. The effect of thermofluid and geometrical parameters on convection of liquids through rectangular microchannels. Int J Heat Mass Transf. 1995;38(4):755–8.
107. Jiang XN, Zhou ZY, Yao J, Li Y, Ye XY. Micro-fluid flow in microchannel. 2005. pp. 317–320.
108. Cuta JM, Bennett WD, McDonald CE, Ravigururajan TS. Fabrication and testing of microchannel heat exchangers. Microlithogr Metrol Micromach. 2004;2640:152–60.
109. Cuta JM, McDonald CE, Shekarriz A. Forced convection heat transfer in parallel channel array microchannel heat exchanger. New York: ASME; 1996.
110. Jiang XN, Zhou ZY, Huang XY, Liu CY. Laminar flow through microchannels used for microscale cooling systems. In: Proceedings of the 1997 1st electronic packaging technology conference (Cat. No. 97TH8307). 2002. pp. 119–122.
111. Harms TM, Kazmierczak MJ, Gerner FM. Developing convective heat transfer in deep rectangular microchannels. Int J Heat Fluid Flow. 1999;20(2):149–57.
112. Tso CP, Mahulikar SP. Multimode heat transfer in two-dimensional microchannel. American Society of Mechanical Engineers, EEP, 26-2. 1999.
113. Vidmar RJ. Microchannel cooling for a high-energy particle transmission window, an RF transmission window, and VLSI heat dissipation. IEEE Trans Plasma Sci. 1998;26(3):1031–43.
114. Adams TM, Abdel-Khalik SI, Jeter SM, Qureshi ZH. An experimental investigation of single-phase forced convection in microchannels. Int J Heat Mass Transf. 1998;41(6–7):851–7.
115. Mala GM, Li D. Flow characteristics of water in microtubes. Int J Heat Fluid Flow. 1999;20(2):142–8.
116. Papautsky I, Brazzle J, Ameel T, Frazier AB. Laminar fluid behavior in microchannels using micropolar fluid theory. Sens Actuators, A Phys. 1999;73(1–2):101–8.
117. Meinhart CD, Wereley ST, Santiago JG. PIV measurements of a microchannel flow. Exp Fluids. 1999;27(5):414–9.
118. Pfund D, Rector D, Shekarriz A, Popescu A, Welty J. Pressure drop measurements in a microchannel. AIChE J. 2000;46(8):1496–507.
119. Qu W, Mala GM, Li D. Heat transfer for water flow in trapezoidal silicon microchannels. Int J Heat Mass Transf. 2000;43(21):3925–36.
120. Qu W, Mohiuddin M, Li D. Pressure-driven water flows in trapezoidal silicon microchannels. Int J Heat Mass Transf. 2000;43(3):353–64.
121. Rahman MM. Measurements of heat transfer in microchannel heat sinks. Int Commun Heat Mass Transf. 2000;27(4):495–506.
122. Ren L, Qu W, Li D. Interfacial electrokinetic effects on liquid flow in microchannels. Int J Heat Mass Transf. 2001;44(16):3125–34.
123. Chung PM-Y, Kawaji M, Kawahara A, Shibata Y. "Two-phase flow through square and circular microchannels: Effect of channel geometry, vol. 1. Fora 2003:1459–1467.
124. Gao P, Le Person S, Favre-Marinet M. Scale effects on hydrodynamics and heat transfer in two-dimensional mini and microchannels. Int J Therm Sci. 2002;41(11):1017–27.
125. Judy J, Maynes D, Webb BW. Characterization of frictional pressure drop for liquid flows through microchannels. Int J Heat Mass Transf. 2002;45(17):3477–89.
126. Lee PS, Ho JC, Xue H. Experimental study on laminar heat transfer in microchannel heat sink. In: ITherm 2002. Eighth intersociety conference on thermal and thermomechanical phenomena in electronic systems (Cat. No. 02CH37258), IEEE; 2002. pp. 379–386.
127. Qu W, Mudawar I. Experimental and numerical study of pressure drop and heat transfer in a single-phase micro-channel heat sink. Int J Heat Mass Transf. 2002;45(12):2549–65.
128. Celata GP, Cumo M, Guglielmi M, Zummo G. Experimental investigation of hydraulic and single-phase heat transfer in 0.130-mm capillary tube. Microscale Thermophys Eng. 2002;6(2):85–97.
129. Li Z-X. Experimental study on flow characteristics of liquid in circular microtubes. Microscale Thermophys Eng. 2003;7(3):253–65.
130. Bucci A, Celata GP, Cumo M, Serra E, Zummo G. Water single-phase fluid flow and heat transfer in capillary tubes. In: 1st international conference on microchannels and minichannels, 2003. pp. 319–326.
131. Jung J-Y, Kwak H-Y. Fluid flow and heat transfer in microchannels with rectangular cross section. Heat Mass Transf. 2008;44(9):1041–9.
132. Lee P-S, Garimella SV. Experimental investigation of heat transfer in microchannels. In: ASME Proceedings, 2008. pp. 391–397.
133. Park H, Pak JJ, Son SY, Lim G, Song I. Fabrication of a microchannel integrated with inner sensors and the analysis of

its laminar flow characteristics. Sens Actuators, A Phys. 2003;103(3):317–29.
134. Tu X, Hrnjak P. Experimental investigation of single-phase flow pressure drop through rectangular microchannels. 2009. pp. 257–267.
135. Wu HY, Cheng P. An experimental study of convective heat transfer in silicon microchannels with different surface conditions. Int J Heat Mass Transf. 2003;46(14):2547–56.
136. Wu HY, Cheng P. Friction factors in smooth trapezoidal silicon microchannels with different aspect ratios. Int J Heat Mass Transf. 2003;46(14):2519–25.
137. Baviere R, Ayela F, Le Person S, Favre-Marinet M. An experimental study of water flow in smooth and rough rectangular micro-channels. 2008, pp. 221–228. http://asmedigitalcollection.asme.org/. Accessed 7 Aug 2019.
138. Hsieh S-S, Lin C-Y, Huang C-F, Tsai H-H. Liquid flow in a micro-channel. J. Micromech Microeng. 2004;14(4):436–45.
139. Lelea D, Nishio S, Takano K. The experimental research on microtube heat transfer and fluid flow of distilled water. Int J Heat Mass Transf. 2004;47(12–13):2817–30.
140. Hao PF, He F, Zhu KQ. Flow characteristics in a trapezoidal silicon microchannel. J Micromech Microeng. 2005;15(6):1362–8.
141. Steinke ME, Kandlikar SG. Single-phase liquid friction factors in microchannels. Int J Therm Sci. 2006;45(11):1073–83.
142. Shen S, Xu JL, Zhou JJ, Chen Y. Flow and heat transfer in microchannels with rough wall surface. Energy Convers Manag. 2006;47(11–12):1311–25.
143. Hrnjak P, Tu X. Single phase pressure drop in microchannels. Int J Heat Fluid Flow. 2007;28(1):2–14.
144. Gamrat G, Favre-Marinet M, Le Person S, Baviere R, Ayela F. An experimental study and modelling of roughness effects on laminar flow in microchannels. J Fluid Mech. 2008;594:399–423.
145. Wibel W, Ehrhard P. Experiments on the laminar/turbulent transition of liquid flows in rectangular microchannels. Heat Transf Eng. 2009;30(1–2):70–7.
146. Mirmanto KDBR, Lewis JS, Karayiannis TG. Pressure drop and heat transfer characteristics for single-phase developing flow of water in rectangular microchannels. J Phys Conf Ser. 2012;395(1):012085.
147. Houshmand F, Peles Y. Convective heat transfer to shear-driven liquid film flow in a microchannel. Int J Heat Mass Transf. 2013;64:42–52.
148. do Nascimento FJ, Leão HLSL, Ribatski G. An experimental study on flow boiling heat transfer of R134a in a microchannel-based heat sink. Exp Therm Fluid Sci. 2013;45:117–27.
149. Balasubramanian K, Lee PS, Teo CJ, Chou SK. Flow boiling heat transfer and pressure drop in stepped fin microchannels. Int J Heat Mass Transf. 2013;67:234–52.
150. Goss G, Passos JC. Heat transfer during the condensation of R134a inside eight parallel microchannels. Int J Heat Mass Transf. 2013;59(1):9–19.
151. Rahimi M, Karimi E, Asadi M, Valeh-e-Sheyda P. Heat transfer augmentation in a hybrid microchannel solar cell. Int Commun Heat Mass Transf. 2013;43:131–7.
152. Roy P, Anand NK, Banerjee D. Liquid slip and heat transfer in rotating rectangular microchannels. Int J Heat Mass Transf. 2013;62(1):184–99.
153. Zhuan R, Wang W. Boiling heat transfer characteristics in a microchannel array heat sink with low mass flow rate. Appl Therm Eng. 2013;51(1–2):65–74.
154. El Mghari H, Asbik M, Louahlia-gualous H, Voicu I. Condensation heat transfer enhancement in a horizontal non-circular microchannel. Appl Therm Eng. 2014;64(1–2):358–70.
155. Chen C, et al. A study on fluid flow and heat transfer in rectangular microchannels with various longitudinal vortex generators. Int J Heat Mass Transf. 2014;69:203–14.
156. Emran M, Islam MA. Numerical investigation of flow dynamics and heat transfer characteristics in a microchannel heat sink. Procedia Eng. 2014;90:563–8.
157. Huang CY, Wu CM, Chen YN, Liou TM. The experimental investigation of axial heat conduction effect on the heat transfer analysis in microchannel flow. Int J Heat Mass Transf. 2014;70:169–73.
158. Law M, Lee PS, Balasubramanian K. Experimental investigation of flow boiling heat transfer in novel oblique-finned microchannels. Int J Heat Mass Transf. 2014;76:419–31.
159. Leão HLSL, do Nascimento FJ, Ribatski G. Flow boiling heat transfer of R407c in a microchannels based heat spreader. Exp Therm Fluid Sci. 2014;59:140–51.
160. Nandi TK, Chattopadhyay H. Numerical investigations of developing flow and heat transfer in raccoon type microchannels under inlet pulsation. Int Commun Heat Mass Transf. 2014;56:37–41.
161. Tan DK, Liu Y. Combined effects of streaming potential and wall slip on flow and heat transfer in microchannels. Int Commun Heat Mass Transf. 2014;53:39–42.
162. Abed WM, Whalley RD, Dennis DJC, Poole RJ. Numerical and experimental investigation of heat transfer and fluid flow characteristics in a micro-scale serpentine channel. Int J Heat Mass Transf. 2015;88:790–802.
163. Chandra AK, Kishor K, Mishra PK, Alam MS. Numerical simulation of heat transfer enhancement in periodic converging-diverging microchannel. Proc Eng. 2015;127:95–101.
164. Dai Z, Fletcher DF, Haynes BS. Impact of tortuous geometry on laminar flow heat transfer in microchannels. Int J Heat Mass Transf. 2015;83:382–98.
165. Dehghan M, Daneshipour M, Valipour MS, Rafee R, Saedodin S. Enhancing heat transfer in microchannel heat sinks using converging flow passages. Energy Convers Manag. 2015;92:244–50.
166. Duryodhan VS, Singh A, Singh SG, Agrawal A. Convective heat transfer in diverging and converging microchannels. Int J Heat Mass Transf. 2015;80:424–38.
167. Ebrahimi A, Roohi E, Kheradmand S. Numerical study of liquid flow and heat transfer in rectangular microchannel with longitudinal vortex generators. Appl Therm Eng. 2015;78:576–83.
168. Guo L, Xu H, Gong L. Influence of wall roughness models on fluid flow and heat transfer in microchannels. Appl Therm Eng. 2015;84:399–408.
169. Lee YJ, Singh PK, Lee PS. Fluid flow and heat transfer investigations on enhanced microchannel heat sink using oblique fins with parametric study. Int J Heat Mass Transf. 2015;81:325–336.
170. Prajapati YK, Pathak M, Kaleem Khan M. A comparative study of flow boiling heat transfer in three different configurations of microchannels. Int J Heat Mass Transf. 2015;85:711–22.
171. Rao SR, Peles Y. Spatiotemporally resolved heat transfer measurements for flow boiling in microchannels. Int J Heat Mass Transf. 2015;89:482–93.
172. Rostami J, Abbassi A, Saffar-Avval M. Optimization of conjugate heat transfer in wavy walls microchannels. Appl Therm Eng. 2015;82:318–28.
173. Vivekanand SVB, Raju VRK. Simulation of evaporation heat transfer in a rectangular microchannel. Proc Eng. 2015;127:309–16.
174. Xia GD, Jiang J, Wang J, Zhai YL, Ma DD. Effects of different geometric structures on fluid flow and heat transfer performance in microchannel heat sinks. Int J Heat Mass Transf. 2015;80:439–47.

175. Zhang L-Y, Zhang Y-F, Chen J-Q, Bai S-L. Fluid flow and heat transfer characteristics of liquid cooling microchannels in LTCC multilayered packaging substrate. Int J Heat Mass Transf. 2015;84:339–45.
176. Chai L, Wang L, Bai X. Thermohydraulic performance of microchannel heat sinks with triangular ribs on sidewalls—part 1: local fluid flow and heat transfer characteristics. Int J Heat Mass Transf. 2018;127:1124–37.
177. Jagirdar M, Lee PS. Study of transient heat transfer and synchronized flow visualizations during sub-cooled flow boiling in a small aspect ratio microchannel. Int J Multiph Flow. 2016;83:254–66.
178. Magnini M, Thome JR. A CFD study of the parameters influencing heat transfer in microchannel slug flow boiling. Int J Therm Sci. 2016;110:119–36.
179. Ma DD, Xia GD, Li YF, Jia YT, Wang J. Effects of structural parameters on fluid flow and heat transfer characteristics in microchannel with offset zigzag grooves in sidewall. Int J Heat Mass Transf. 2016;101:427–35.
180. Prajapati YK, Pathak M, Khan MK. Transient heat transfer characteristics of segmented finned microchannels. Exp Therm Fluid Sci. 2016;79:134–42.
181. Sahar AM, Özdemir MR, Fayyadh EM, Wissink J, Mahmoud MM, Karayiannis TG. Single phase flow pressure drop and heat transfer in rectangular metallic microchannels. Appl Therm Eng. 2016;93:1324–36.
182. Xu S, Li Y, Hu X, Yang L. Characteristics of heat transfer and fluid flow in a fractal multilayer silicon microchannel. Int Commun Heat Mass Transf. 2016;71:86–95.
183. Yang F, Li W, Dai X, Li C. Flow boiling heat transfer of HFE-7000 in nanowire-coated microchannels. Appl Therm Eng. 2016;93:260–8.
184. Dalkılıç AS, Mahian O, Yılmaz S, Sakamatapan K, Wongwises S. Experimental investigation of single-phase turbulent flow of R-134a in a multiport microchannel heat sink. Int Commun Heat Mass Transf. 2017;89:47–56.
185. Feng Z, Luo X, Guo F, Li H, Zhang J. Numerical investigation on laminar flow and heat transfer in rectangular microchannel heat sink with wire coil inserts. Appl Therm Eng. 2017;116:597–609.
186. Ghani IA, Kamaruzaman N, Sidik NAC. Heat transfer augmentation in a microchannel heat sink with sinusoidal cavities and rectangular ribs. Int J Heat Mass Transf. 2017;108:1969–81.
187. Sahar AM, Wissink J, Mahmoud MM, Karayiannis TG, Ishak MSA. Effect of hydraulic diameter and aspect ratio on single phase flow and heat transfer in a rectangular microchannel. Appl Therm Eng. 2017;115:793–814.
188. Wan Z, Lin Q, Wang X, Tang Y. Flow characteristics and heat transfer performance of half-corrugated microchannels. Appl Therm Eng. 2017;123:1140–51.
189. Zhang Y, Wang J, Liu W, Liu Z. Heat transfer and pressure drop characteristics of R134a flow boiling in the parallel/tandem microchannel heat sinks. Energy Convers Manag. 2017;148:1082–95.
190. Zhou F, Zhou W, Qiu Q, Yu W, Chu X. Investigation of fluid flow and heat transfer characteristics of parallel flow double-layer microchannel heat exchanger. Appl Therm Eng. 2018;137:616–31.
191. Wang SL, Li XY, Wang XD, Lu G. Flow and heat transfer characteristics in double-layered microchannel heat sinks with porous fins. Int Commun Heat Mass Transf. 2018;93:41–7.
192. Li P, Luo Y, Zhang D, Xie Y. Flow and heat transfer characteristics and optimization study on the water-cooled microchannel heat sinks with dimple and pin-fin. Int J Heat Mass Transf. 2018;119:152–62.
193. Esmaili Q, Ranjbar AA, Porkhial S. Experimental analysis of heat transfer in ribbed microchannel. Int J Therm Sci. 2018;130(April):140–7.
194. Choi SB, Barron RF, Warrington RO. Fluid flow and heat transfer in microtubes. Micromech Sens Actuators Syst. 1991;32:123–34.
195. Pong KC, Ho CM, Liu J, Tai YC. Non-linear pressure distribution in uniform microchannels. Am Soc Mech Eng Fluids Eng Div FED. 1994;197:51.
196. Arkilic EB, Schmidt MA, Breuer KS. Gaseous slip flow in long microchannels. J. Microelectromech Syst. 1997;6(2):167–78.
197. Shih JC, Ho C-M, Liu J, Tai Y-C. Monatomic and polyatomic gas flow through uniform microchannels. Am Soc Mech Eng Dyn Syst Control Div DSC. 1996;59:197–203.
198. Stanley R, Ameel T, Barron R. Two-phase flow in microchannels. 1997.
199. Wu S, Mai J, Zohar Y, Tai YC, Ho CM. A suspended microchannel with integrated temperature sensors for high-pressure flow studies. 2002. pp. 87–92. http://ieeexplore.ieee.org/. Accessed 7 Aug 2019.
200. Araki T, Kim MS, Iwai H, Suzuki K. An experimental investigation of gaseous flow characteristics in microchannels. Microscale Thermophys Eng. 2002;6(2):117–30.
201. Turner SE, Sun H, Faghri M, Gregory OJ. Compressible gas flow through smooth and rough microchannels. In: ASME-PUBLICATIONS-HTD, 2001, vol. 369, pp. 381–384.
202. Asako Y, Nakayama K, Shinozuka T. Effect of compressibility on gaseous flows in a micro-tube. Int J Heat Mass Transf. 2005;48(23–24):4985–94.
203. Kohl MJ, Abdel-Khalik SI, Jeter SM, Sadowski DL. An experimental investigation of microchannel flow with internal pressure measurements. Int J Heat Mass Transf. 2005;48(8):1518–33.
204. Tang GH, Li Z, He YL, Tao WQ. Experimental study of compressibility, roughness and rarefaction influences on microchannel flow. Int J Heat Mass Transf. 2007;50(11–12):2282–95.
205. Morini GL, Lorenzini M, Salvigni S, Spiga M. Analysis of laminar-to-turbulent transition for isothermal gas flows in microchannels. Microfluid Nanofluidics. 2009;7(2):181–90.
206. Vijayalakshmi K, Anoop KB, Patel HE, Harikrishna PV, Sundararajan T, Das SK. Effects of compressibility and transition to turbulence on flow through microchannels. Int J Heat Mass Transf. 2009;52(9–10):2196–204.
207. Chen L, Zhang XR. Heat transfer and various convection structures of near-critical CO_2 flow in microchannels. Appl Therm Eng. 2014;72(1):135–42.
208. Yuan X, Tao Z, Li H, Tian Y. Experimental investigation of surface roughness effects on flow behavior and heat transfer characteristics for circular microchannels. Chin J Aeronaut. 2016;29(6):1575–81.
209. Kim B. An experimental study on fully developed laminar flow and heat transfer in rectangular microchannels. Int J Heat Fluid Flow. 2016;62:224–32.
210. Ding L, Sun H, Sheng XL, Lee BD. Measurement of friction factor for R134a and R12 through microchannels. In: Proceedings of symposium on energy engineering in the 21st century. 2000, vol. 2, pp. 650–657.
211. Cioncolini A, Thome JR, Lombardi C. Unified macro-to-microscale method to predict two-phase frictional pressure drops of annular flows. Int J Multiph Flow. 2009;35(12):1138–48.
212. Jiang PX, Fan MH, Si GS, Ren ZP. Thermal-hydraulic performance of small scale micro-channel and porous-media heat-exchangers. Int J Heat Mass Transf. 2001;44(5):1039–51.
213. Sharp KV, Adrian RJ. Transition from laminar to turbulent flow in liquid filled microtubes. Exp Fluids. 2004;36(5):741–7.

214. Wang BX, Peng XF. Experimental investigation on liquid forced-convection heat transfer through microchannels. Int J Heat Mass Transf. 1994;37(SUPPL. 1):73–82.
215. Schilder B, Man SYC, Kasagi N, Hardt S, Stephan P. Flow visualization and local measurement of forced convection heat transfer in a microtube. J Heat Transf. 2010;132(3):031702.
216. Gnielinski V. New equations for heat and mass transfer in the turbulent flow in pipes and channels. Forsch Im Ingenieurwes. 1975;41(1):10.
217. Garimella SV, Singhal V. Single-phase flow and heat transport and pumping considerations in microchannel heat sinks. Heat Transf Eng. 2004;25(1):15–25.
218. Silvério V, Moreira ALN. Friction losses and heat transfer in laminar microchannel single-phase liquid flow. 2009. pp. 259–267. http://asmedigitalcollection.asme.org/. Accessed 12 Aug 2019.
219. Kays WM. Convective heat and mass transfer. New York: Tata McGraw-Hill Education; 2012.
220. Incropera FP, Lavine AS, Bergman TL, DeWitt DP. Fundamentals of heat and mass transfer. 2007.
221. Stephan K, Preußer P. Wärmeübergang und maximale Wärmestromdichte beim Behältersieden binärer und ternärer Flüssigkeitsgemische. Chemie Ing Tech. 1979;51(1):37.
222. Shah RK, London AL. Laminar flow forced convection in ducts: a source book for compact heat exchanger analytical data. Cambridge: Academic Press; 2014.
223. Kakaç S, Shah RK, Aung W. Handbook of single-phase convective heat transfer. 1987.
224. Yu D, Warrington R, Barron R, Ameel T. An experimental and theoretical investigation of fluid flow and heat transfer in microtubes. ASME/JSME Therm Eng Conf. 1995;1(52):523–30.
225. Grigull U, Tratz H. Thermischer einlauf in ausgebildeter laminarer rohrströmung. Int J Heat Mass Transf. 1965;8(5):669–78.
226. Bejan A. Convection heat transfer. Wiley; 2013.
227. Şen S, Darici S. Transient conjugate heat transfer in a circular microchannel involving rarefaction, viscous dissipation and axial conduction effects. Appl Therm Eng. 2017;111:855–62.
228. Fayyadh EM, Mahmoud MM, Sefiane K, Karayiannis TG. Flow boiling heat transfer of R134a in multi microchannels. Int J Heat Mass Transf. 2017;110:422–36.
229. Debray F, Franc JP, Maître T, Reynaud S. Mesure des coefficients de transfert thermique par convection forcée en mini-canaux. Mec Ind. 2001;2(5):443–54.
230. Che Z, Wong TN, Nguyen NT, Yang C. Three dimensional features of convective heat transfer in droplet-based microchannel heat sinks. Int J Heat Mass Transf. 2015;86:455–64.
231. Fischer M, Juric D, Poulikakos D. Large convective heat transfer enhancement in microchannels with a train of coflowing immiscible or colloidal droplets. J Heat Transf. 2010;132(11):112402.
232. Hasan AR, Kabir CS, Sarica C. Fluid flow and heat transfer in wellbores. 2002. p. 181. https://ci.nii.ac.jp/. Accessed 13 Aug 2019.
233. Chu J-C, Teng J-T, Greif R. heat transfer for water flow in triangular silicon microchannels. J Therm Sci Technol. 2008;3(3):410–20.
234. Ravigururajan TS. Impact of channel geometry on two-phase flow heat transfer characteristics of refrigerants in microchannel heat exchangers. J Heat Transfer. 1998;120(2):485.
235. Acosta RE, Muller RH, Tobias CW. Transport processes in narrow (capillary) channels. AIChE J. 1985;31(3):473–82.
236. Bucci A, Celata GP, Cumo M, Serra E, Zummo G. Water single-phase fluid flow and heat transfer in capillary tubes. 2009. pp. 319–326. http://asmedigitalcollection.asme.org/. Accessed 18 Aug 2019.
237. Morini GL. Scaling effects for liquid flows in microchannels. Heat Transf Eng. 2006;27(731700955):64–73.
238. Rosa P, Karayiannis TG, Collins MW. Single-phase heat transfer in microchannels: the importance of scaling effects. Appl Therm Eng. 2009;29(17–18):3447–68.
239. Costa-Patry E, Olivier J, Michel B, Thome JR. Two-phase flow of refrigerants in 85 μm-wide multi-microchannels: part II—heat transfer with 35 local heaters. Int J Heat Fluid Flow. 2011;32(2):464–76.
240. McAdams WH. Vaporization inside horizontal tubes-II, Benzene oil mixtures. Trans. ASME. 1942;64:193–200.
241. Owens WL. Two-phase pressure gradient. In: International development in heat transfer. 1961.
242. Cicchitti A, Lombardi C, Silvestri M, Soldaini G, Zavattarelli R. Two-phase cooling experiments: pressure drop, heat transfer and burnout measurements. No. CISE-71. Milan: Centro Informazioni Studi Esperienze; 1959.
243. Dukler AE, Wicks M, Cleveland RG. Frictional pressure drop in two-phase flow: B. An approach through similarity analysis. AIChE J. 1964;10(1):44–51.
244. Beattie DRH, Whalley PB. A simple two-phase frictional pressure drop calculation method. Int J Multiph Flow. 1982;8(1):83–7.
245. Awad MM, Muzychka YS. Bounds on two-phase frictional pressure gradient in minichannels and microchannels. Heat Transf Eng. 2007;28(8–9):720–9.
246. Venkatesan M, Das SK, Balakrishnan AR. Effect of diameter on two-phase pressure drop in narrow tubes. Exp Therm Fluid Sci. 2011;35(3):531–41.
247. Choi C, Kim M. Flow pattern based correlations of two-phase pressure drop in rectangular microchannels. Int J Heat Fluid Flow. 2011;32(6):1199–207.
248. Liu H, Vandu CO, Krishna R. Hydrodynamics of taylor flow in vertical capillaries: flow regimes, bubble rise velocity, liquid slug length, and pressure drop. Ind Eng Chem Res. 2005;44(14):4884–97.
249. Mishima K, Hibiki T. Some characteristics of air–water two-phase flow in small diameter vertical tubes. Int J Multiph Flow. 1996;22(4):703–12.
250. Zhang M, Webb RL. Correlation of two-phase friction for refrigerants in small-diameter tubes. Exp Therm Fluid Sci. 2001;25(3–4):131–9.
251. Lee HJ, Lee SY. Pressure drop correlation for two-phase flow within horizontal rectangular channels with small heights. Int J Multiph Flow. 2001;27(5):783–96.
252. Chen JC. Correlation for boiling heat transfer to saturated fluids in convective flow. Ind Eng Chem Process Des Dev. 1966;5(3):322–9.
253. Qu W, Mudawar I. Measurement and prediction of pressure drop in two-phase micro-channel heat sinks. Int J Heat Mass Transf. 2003;46(15):2737–53.
254. Yue J, Chen G, Yuan Q. Pressure drops of single and two-phase flows through T-type microchannel mixers. Chem Eng J. 2004;102(1):11–24.
255. Coleman JW, Krause PE. Two phase pressure losses of R134a in microchannel tube headers with large free flow area ratios. Exp Therm Fluid Sci. 2004;28(2–3):123–30.
256. Chung PM-Y, Kawaji M, Kawahara A, Shibata Y. Two-phase flow through square and circular microchannels—effects of channel geometry. J Fluids Eng. 2004;126(4):546.
257. Lee J, Mudawar I. Two-phase flow in high-heat-flux micro-channel heat sink for refrigeration cooling applications: part I—pressure drop characteristics. Int J Heat Mass Transf. 2005;48(5):928–40.

258. Pamitran AS, Choi KI, Oh JT, Oh HK. Two-phase pressure drop during CO_2 vaporization in horizontal smooth minichannels. Int J Refrig. 2008;31(8):1375–83.
259. Yue J, Luo L, Gonthier Y, Chen G, Yuan Q. An experimental investigation of gas–liquid two-phase flow in single microchannel contactors. Chem Eng Sci. 2008;63(16):4189–202.
260. Lee P-S, Garimella SV. Experimental investigation of heat transfer in microchannels. In: ASME conference proceedings. 2008. pp. 391–397.
261. Choi KI, Pamitran AS, Oh CY, Oh JT. Two-phase pressure drop of R-410A in horizontal smooth minichannels. Int J Refrig. 2008;31(1):119–29.
262. Li X, Hibiki T. Frictional pressure drop correlation for two-phase flows in mini and micro multi-channels. Appl Therm Eng. 2017;116:316–28.
263. Kawahara A, Chung PY, Kawaji M. Investigation of two-phase flow pattern, void fraction and pressure drop in a microchannel. Int J Multiph Flow. 2002;28(9):1411–35.
264. Megahed A, Hassan I. Two-phase pressure drop and flow visualization of FC-72 in a silicon microchannel heat sink. Int J Heat Fluid Flow. 2009;30(6):1171–82.
265. Lee HJ, Liu DY, Alyousef Y, Yao S. Generalized two-phase pressure drop and heat transfer correlations in evaporative micro/minichannels. J Heat Transf. 2010;132(4):041004.
266. Garcia J, Porto MP, Revellin R, Bonjour J, Machado L. An experimental study on two-phase frictional pressure drop for R-407c in smooth horizontal tubes. Int J Refrig. 2016;73:163–74.
267. Zhao TS, Bi QC. Pressure drop characteristics of gas–liquid two-phase flow in vertical miniature triangular channels. Int J Heat Mass Transf. 2001;44(13):2523–34.
268. Lockhart RW, Martinelli RC. Proposed correlation of data for isothermal two-phase two component flow in pipes. Chem Eng Prog. 1949;45:39–48.
269. Friedel L. Improved friction pressure drop correlation for horizontal and vertical two-phase pipe flow. In: Proceeding of European Two-Phase Flow Group Meet, 1979.
270. Fukano T, Kariyasaki A. Characteristics of gas–liquid two-phase flow in a capillary tube. Nucl Eng Des. 1993;141(1–2):59–68.
271. Cavallini A, Del Col D, Doretti L, Matkovic M, Rossetto L, Zilio C. Two-phase frictional pressure gradient of R236ea, R134a and R410a inside multi-port mini-channels. Exp Therm Fluid Sci. 2005;29(7):861–70.
272. Chisholm D. A theoretical basis for the Lockhart–Martinelli correlation for two-phase flow. Int J Heat Mass Transf. 1967;10(12):1767–78.
273. Müller-Steinhagen H, Heck K. A simple friction pressure drop correlation for two-phase flow in pipes. Chem Eng Process. 1986;20(6):297–308.
274. Ong CL, Thome JR. Macro-to-microchannel transition in two-phase flow: part 1—two-phase flow patterns and film thickness measurements. Exp Therm Fluid Sci. 2011;35(1):37–47.
275. Rapolu P, Son SY. Characterization of wettability effects on pressure drop of two-phase flow in microchannel. Exp Fluids. 2011;51(4):1101–8.
276. Kozulin IA, Kuznetsov VV. Statistical characteristics of two-phase gas–liquid flow in a vertical microchannel. J Appl Mech Tech Phys. 2011;52(6):956–64.
277. Adams DC, Burr J, Hrnjak P, Newell T. Two phase pressure drop of CO_2, ammonia, and R245fa in multiport aluminum microchannel tubes.
278. Tran TN, Chyu MC, Wambsganss MW, France DM. Two-phase pressure drop of refrigerants during flow boiling in small channels: an experimental investigation and correlation development. Int J Multiph Flow. 2000;26(11):1739–54.
279. Li W, Wu Z. A general correlation for evaporative heat transfer in micro/mini-channels. Int J Heat Mass Transf. 2010;53(9–10):1778–87.
280. Forster HK, Zuber N. Dynamics of vapor bubbles and boiling heat transfer. AIChE J. 1955;1(4):531–5.
281. Kandlikar SG. A general correlation for saturated two-phase flow boiling heat transfer inside horizontal and vertical tubes. J Heat Transf. 1990;112(1):219.
282. Gungor KE, Winterton RHS. A general correlation for flow boiling in tubes and annuli. Int J Heat Mass Transf. 1986;29(3):351–8.
283. Shah RK, London AL. Rectangular ducts. In: Laminar flow forced convection ducts. 1978. pp. 196–222.
284. Lazarek GM, Black SH. Evaporative heat transfer, pressure drop and critical heat flux in a small vertical tube with R-113. Int J Heat Mass Transf. 1982;25(7):945–60.
285. Cornwell K, Kew PA. Boiling in small parallel channels. In: Energy efficiency in process technology. Dordrecht: Springer Netherlands. 1993. p. 624–38.
286. Moriyama K, Inoue A, Ohira H. The thermohydraulic characteristics of two-phase flow in extremely narrow channels (the frictional pressure drop and heat transfer boiling two-phase flow, analytical model). Heat Transf-Jpn Res. 1993;21(8):838–56.
287. Bowers MB, Mudawar I. High flux boiling in low flow rate, low pressure drop mini-channel and micro-channel heat sinks. Int J Heat Mass Transf. 1994;37(2):321–32.
288. Wambsganss MW, France DM, Jendrzejczyk JA, Tran TN. Boiling heat transfer in a horizontal small-diameter tube. J Heat Transf. 2008;115(4):963.
289. Mertz R, Wein A, Groll M. Experimental investigation of flow boiling heat transfer in narrow channels. Heat Technol. 1996;14(2):47–54.
290. Kew PA, Cornwell K. Correlations for the prediction of boiling heat transfer in small diameter channels. Appl Therm Eng. 1997;17:705–15.
291. Mehendale SS, Jacobi AM. Evaporative heat transfer in mesoscale heat exchangers. 2000.
292. Zhao Y, Chen G, Yuan Q. Liquid–liquid two-phase flow patterns in a rectangular microchannel. AIChE J. 2006;52(12):4052–60.
293. Agostini B, et al. High heat flux flow boiling in silicon multi-microchannels: part III—saturated critical heat flux of R236fa and two-phase pressure drops. Int J Heat Mass Transf. 2008;51(21–22):5426–42.
294. Ergu OB, Sara ON, Yapici S, Arzutug ME. Pressure drop and point mass transfer in a rectangular microchannel. Int Commun Heat Mass Transf. 2009;36(6):618–23.
295. Alapati S, Kang S, Suh YK. Parallel computation of two-phase flow in a microchannel using the lattice Boltzmann method. J Mech Sci Technol. 2009;23(9):2492–501.
296. Na YW, Chung JN. Two-phase annular flow and evaporative heat transfer in a microchannel. Int J Heat Fluid Flow. 2011;32(2):440–50.
297. Autee AT, Srinivasa Rao S, Ravikumar P, Shrivastava RK. Two-phase pressure drop calculations in small diameter inclined tubes. Int J Eng Technol. 2012;1(3):168–81.
298. Ide H, Kimura R, Hashiguchi H, Kawaji M. Effect of channel length on the gas–liquid two-phase flow phenomena in a microchannel. Heat Transf Eng. 2012;33(3):225–33.
299. Szczukiewicz S, Magnini M, Thome JR. Proposed models, ongoing experiments, and latest numerical simulations of microchannel two-phase flow boiling. Int J Multiph Flow. 2014;59:84–101.
300. Houshmand F, Peles Y. Heat transfer enhancement with liquid–gas flow in microchannels and the effect of thermal boundary layer. Int J Heat Mass Transf. 2014;70:725–33.

301. Suwankamnerd P, Wongwises S. An experimental study of two-phase air-water flow and heat transfer characteristics of segmented flow in a microchannel. Exp Therm Fluid Sci. 2015;62:29–39.
302. Chinnov EA, Ron'shin FV, Kabov OA. Two-phase flow patterns in short horizontal rectangular microchannels. Int J Multiph Flow. 2016;80:57–68.
303. Vanderputten MA, Jacob TA, Sattar M, Ali N, Fronk BM. Two-phase flow regimes of condensing R-134a at low mass flux in rectangular microchannels. Int J Refrig. 2017;84:92–103.
304. Dalkılıç AS, Özman C, Sakamatapan K, Wongwises S. Experimental investigation on the flow boiling of R134a in a multi-microchannel heat sink. Int Commun Heat Mass Transf. 2018;91:125–37.